U N I V E R S I T Y O F T A S M A N I A

THE MAGNETO-IONIC TRIPLE SPLITTING OF IONOSPHERIC ECHOES

by

G. R. ELLIS

[A thesis presented for the degree of Ph.D. in the University of Tasmania].

[1955].

CONTENTS.

1. INTRODUCTION.

In 1933 T. L. Eckersley (1) observed F region ionospheric echoes which appeared to be magneto-ionically split into three components instead of the usual two. The occurrence of such triple splitting was not reported again until 1936 when Toshniwal (2) in Allahabad and Harang (3) in Tromso both observed similar phenomena. Harang was the first to publish a P'f curve of the echo structure which showed beyond doubt that the third or Z echo was of magneto-ionic origin and that it had the following characteristics:

(i) The critical frequency was approximately $\frac{f_H}{2}$ # less than that of the ordinary echo and f_H less than that of the extraordinary echo.

(ii) In the absence of an F_1 layer, at a given frequency the heights of the three types of echoes were in the order X, O, Z upwards.

(iii) The Z echo was weak compared with O and X echoes.

These features made it probable that Z echoes were due to reflection at the third possible level predicted by the Appleton-Hartree magnetic-ionic theory. However, as we shall discuss in detail later, this theory which explains all the major features of ionospheric propagation, does not predict the simultaneous occurrence of three echoes at vertical incidence. The anomaly was recognised by many workers and several alternative suggestions and theories were advanced to account for it. None was conclusive, mainly because of insufficient experimental information.

During the war, when high latitude ionospheric stations were set up at a number of places, it became obvious that triple splitting was a normal, if infrequent, feature of ionospheric observations at medium and high magnetic latitudes. Reports from Meek (4), Seaton (5) and Scott (6) in Canada, Newstead (7) in Tasmania and Rydbeck (8) in Norway showed that the minimum magnetic latitude for regular observation was about 54° with a corresponding maximum inclination of the geomagnetic field of about 20°. Typical figures for the occurrence of triple splitting at three places in northern Canada are given in Table 1.

The symbols used in Sections 1 and 2 are given on page 4.

Such widespread observations made the problem of triple splitting one of considerable interest. However, even by 1951 there was still no generally accepted theory and the present investigation was initiated as an attempt to find the correct explanation. Some P'f records of triple splitting are shown in Figs. 1 and 2.

Table 1.

Place	Position	Geomagnetic Latitude	Dip	Percentage occurrence of Triple Splitting.	
Clyde	70°N.70°W.	82°N.	84°20'	1.7%	1946
Churchill	58°N.94°W.	70°N.	84°	6.4%	1946
Portage	49.9°N.98°W.	62°N.	78°20'	1.6%	1947

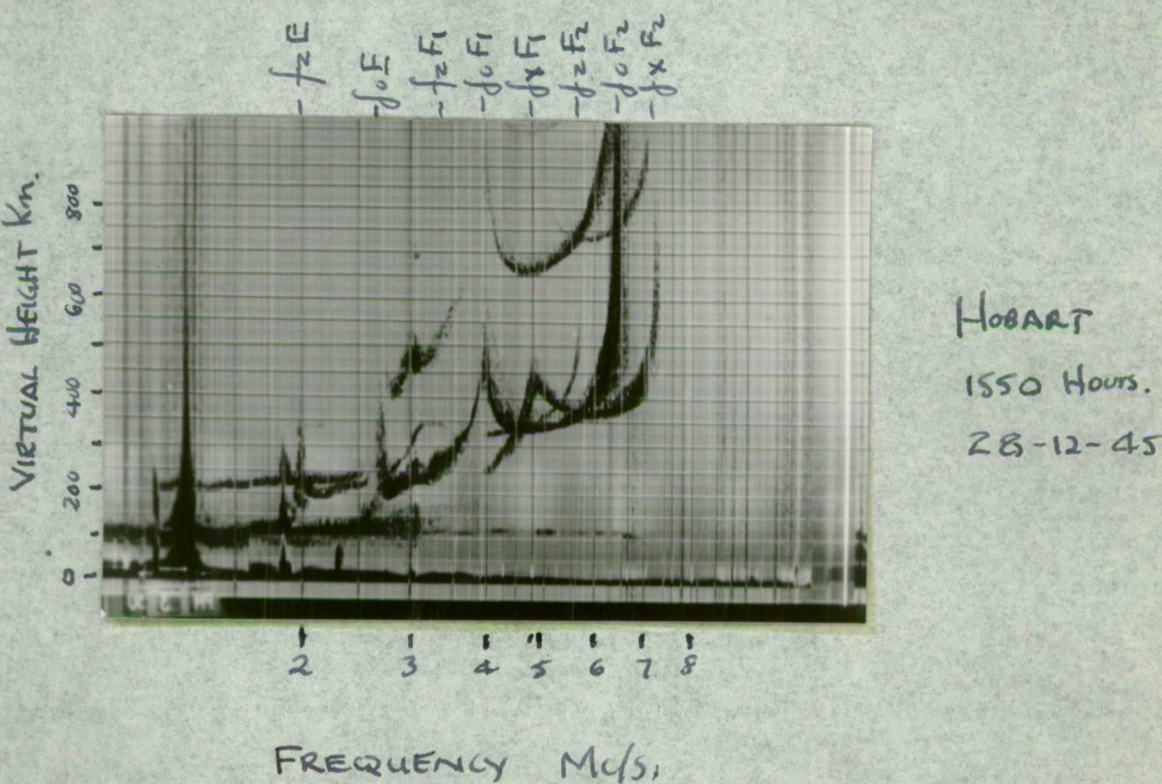

FIG. 1.

Hobart. Geographic Co-ordinates 147.5°E. 42.9°S.

Geomagnetic Co-ordinates 224.6°E. 51.7°S.

Magnetic Elements H = .185 gauss

Z = .565 gauss

Dip 72°

Magnetic Variation 10.5°E.

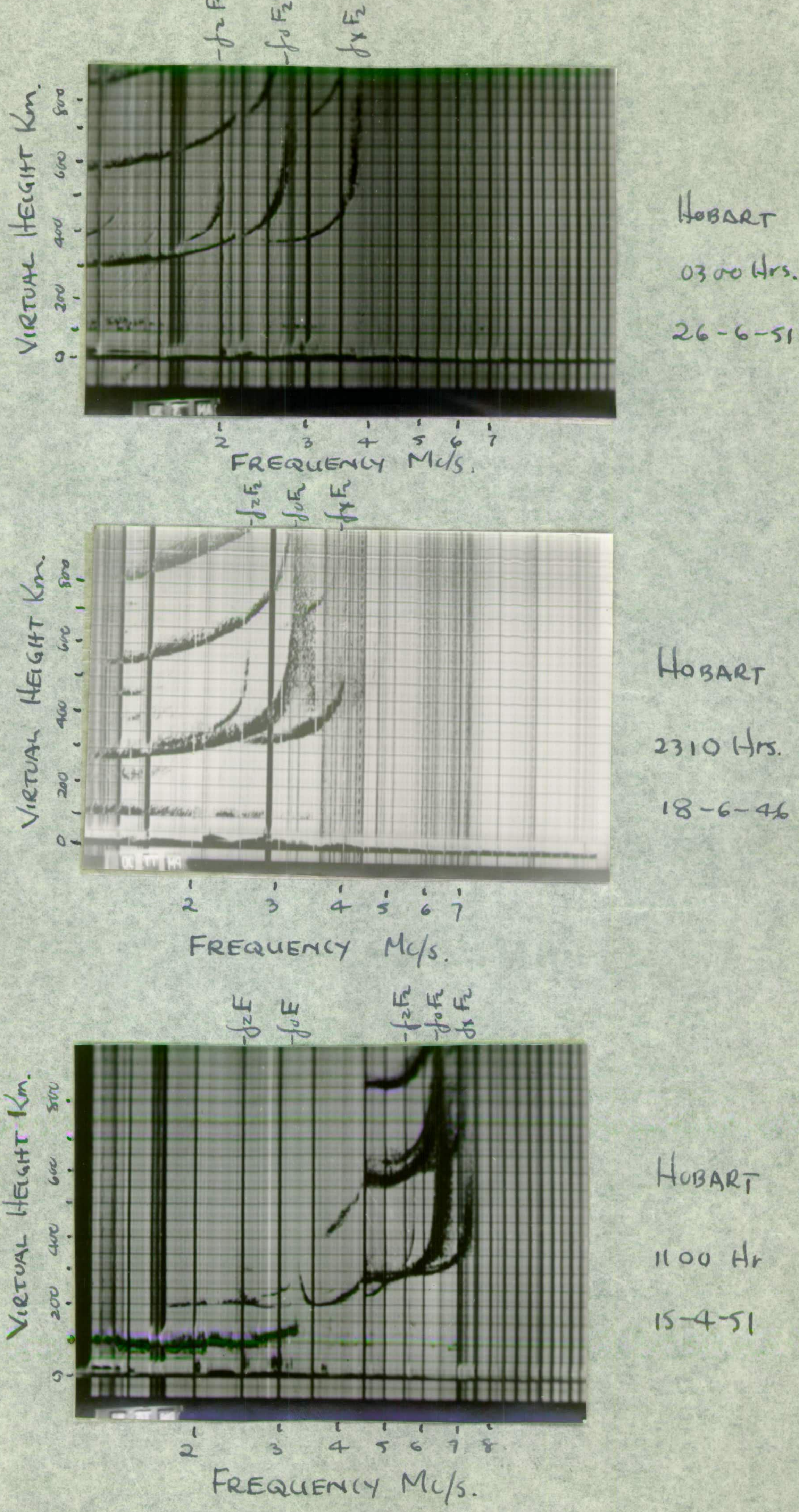
f_zF_2
f_oF_2
f_xF_2
Virtual Height Km.
0
200
400
600
800
2
3
4
5
6
7
Frequency Mc/s.
Hobart
0300 Hrs.
26-6-51
f_zF_2
f_oF_2
f_xF_2
Virtual Height Km.
0
200
400
600
800
2
3
4
5
6
7
Frequency Mc/s.
Hobart
2310 Hrs.
18-6-46
f_zE
f_oE
f_zF_2
f_oF_2
f_xF_2
Virtual Height Km.
0
200
400
600
800
2
3
4
5
6
7
8
Frequency Mc/s.
Hobart
1100 Hr
15-4-51

Figure 2.

LIST OF SYMBOLS

e = charge of electron

m = mass of electron

c = velocity of electromagnetic waves in free space

H_o = intensity of the earth's magnetic field

Θ_o = inclination of the earth's magnetic field to the vertical

f_H = $\frac{eH_o}{2\pi mc} = \frac{p_H}{2\pi}$ = gyro frequency of electrons in the ionosphere

ν = collision frequency of electrons in the ionosphere

N = density of electrons in the ionosphere

N_{max} = maximum electron density

p = angular wave frequency

$p_o^2 = \frac{4\pi N e^2}{m}$

Θ = propagation angle. The angle between the direction of the earth's magnetic field and the direction of the wave normal.

$\gamma = \frac{p p_H}{p_o^2}$

$\gamma_L = \frac{p p_H}{p_o^2} \cos\Theta$

$\gamma_T = \frac{p p_H}{p_o^2} \sin\Theta$

f_z = critical frequency of z wave

f_o = critical frequency of ordinary wave

f_x = critical frequency of extraordinary wave

$p_L = p \cos\Theta$

$p_T = p \sin\Theta$

2. REVIEW OF THEORIES OF TRIPLE SPLITTING.

2.1 Fundamental Theory.

The basic equations of propagation in an ionised medium have been treated in detail by many authors, see for example (9), (10), (11), (12). In this section we shall review some of the fundamentals of the theory.

The displacement $\bar{r}$ of an electron in an ionised medium under the influence of an electric field $\bar{E}$ and magnetic field $\bar{H}_0$ is given by the equations of motion:

$$m\ddot{\bar{r}} = -e\bar{E} - m\nu\dot{\bar{r}} - \frac{e}{c}\dot{\bar{r}}\times\bar{H}_0 \qquad (1)$$

We have assumed here that the wave magnetic intensity $\bar{H}$ is small compared with the geomagnetic field intensity $\bar{H}_0$. This assumption is justified in the case of the ionosphere and has the effect of making the relation linear. We have also neglected the contribution by positive ions and have taken the Lorentz polarisation term to be zero.

Introducing the polarisation vector through the relation

$$\bar{P} = Ne\bar{r} \qquad (2)$$

equation (1) becomes:

$$Nem\ddot{\bar{P}} = -e\bar{E} - m\nu Ne\dot{\bar{P}} - \frac{e^2}{c} N\dot{\bar{P}}\times\bar{H}_0 \qquad (3)$$

Maxwell's equations of the wave field are given by

$$\begin{aligned} \mathrm{curl}\,\bar{H} &= \frac{1}{c}\dot{\bar{D}} \qquad & \mathrm{div}\,\bar{D} &= 0 \\ \mathrm{curl}\,\bar{E} &= -\frac{1}{c}\dot{\bar{H}} \qquad & \mathrm{div}\,\bar{H} &= 0 \end{aligned} \qquad (4)$$

which may be reduced to

$$\nabla^2\bar{E} - \mathrm{grad}\,\mathrm{div}\,\bar{E} - \frac{1}{c^2}\left(\ddot{\bar{E}} + 4\pi\ddot{\bar{P}}\right) = 0 \qquad (5)$$

Equations (3) and (5) determine the electromagnetic field in the medium completely. Since they are linear and homogeneous it is sufficient to consider only harmonic time variations of the field. We choose a rectangular system of co-ordinates x,y,z with the geomagnetic field in the y,z plane. Equation (3) may then be written: time factor e^{ipt}

$$\begin{aligned} E_x &= -4\pi\left[\frac{p_0^2}{p^2}\left(1-\frac{i\nu}{p}\right)P_x - i\gamma_L P_y - i\gamma_T P_z\right] \\ E_y &= -4\pi\left[i\gamma_L P_x + \frac{p^2}{p_0^2}\left(1-\frac{i\nu}{p}\right)P_y\right] \\ E_z &= -4\pi\left[i\gamma_T P_x + \frac{p^2}{p_0^2}\left(1-\frac{i\nu}{p}\right)P_z\right] \end{aligned} \qquad (6)$$

or $\bar{E} = \bar{\lambda}\bar{P}$ where $\bar{\lambda}$ may be called the polarisation tensor. By introducing the dielectric displacement vector $\bar{D} = \bar{E} + 4\pi\bar{P}$ we can obtain the equivalent relation $\bar{D} = \bar{\epsilon}\bar{E}$ where $\bar{\epsilon}$ is the dielectric tensor. If the direction of wave propagation is along the z axis and the medium is either uniform or stratified normal to z, we may put

$$\frac{\partial}{\partial x} = \frac{\partial}{\partial y} = 0$$

The condition $\mathrm{div}\,\bar{D} = 0$ then implies that

$$D_z = E_z + 4\pi P_z \tag{7}$$

Under these conditions the six equations of (5) and (6) may be reduced to the following four:

$$\left.\begin{aligned} E_x &= -4\pi\left[\left(\frac{p_0^2}{p^2}\left(1-\frac{i\nu}{p}\right) + \frac{p_T^2}{1-\frac{p^2}{p_0^2}\left(1-\frac{i\nu}{p}\right)}\right)P_x - i p_L P_y\right] \\ E_y &= -4\pi\left[\quad i p_L P_x + \frac{p^2}{p_0^2}\left(1-\frac{i\nu}{p}\right)P_y\right] \end{aligned}\right\} \quad 8(a)$$

$$\left.\begin{aligned} \frac{\partial^2 E_x}{\partial z^2} &+ \frac{p^2}{c^2}\left(E_x + 4\pi P_x\right) = 0 \\ \frac{\partial^2 E_y}{\partial z^2} &+ \frac{p^2}{c^2}\left(E_y + 4\pi P_y\right) = 0 \end{aligned}\right\} \quad 8(b)$$

These are the basic magneto-ionic equations of propagation in a uniform ionised medium or of vertical incidence propagation in a horizontally stratified ionised medium (taking the z direction to be vertically upwards).

2.2 Ray Theory for a Slowly Varying Medium.

Let the electric intensity of the electro-magnetic wave be represented by the function

$$\bar{E} = \bar{E}_0\, e^{ip\left(t - \frac{nz}{c}\right)} \tag{9}$$

This expression defines n the refractive index by the velocity of phase propagation. If the medium is slowly varying, that is

$$\frac{\partial(nz)}{\partial z} \sim n \qquad \frac{\partial^2 n}{\partial z^2} \text{ and } \left(\frac{\partial n}{\partial z}\right)^2 \text{ negligible}$$

equations (8) and (9) may be reduced to

$$\left[\frac{1}{1-n^2} - \frac{p^2}{p_0^2}\left(1-\frac{i\nu}{p}\right) + \frac{\gamma_T^2}{1-\frac{p^2}{p_0^2}\left(1-\frac{i\nu}{p}\right)}\right] P_x + i\gamma_L P_y = 0$$

$$-i\gamma_L P_x + \left(\frac{1}{1-n^2} - \frac{p^2}{p_0^2}\left(1-\frac{i\nu}{p}\right)\right) P_y = 0 \qquad (10)$$

The condition that these two equations are consistent is that the determinant of their coefficients is zero, that is:

$$\left[\frac{1}{1-n^2} - \frac{p^2}{p_0^2}\left(1-\frac{i\nu}{p}\right) + \frac{\gamma_T^2}{1-\frac{p^2}{p_0^2}\left(1-\frac{i\nu}{p}\right)}\right]\left[\frac{1}{1-n^2} - \frac{p^2}{p_0^2}\left(1-\frac{i\nu}{p}\right)\right] - \gamma_L^2 = 0 \qquad (11)$$

that is:

$$\frac{1}{(1-n^2)^2} + \left\{\frac{\gamma_T^2}{1-\frac{p^2}{p_0^2}\left(1-\frac{i\nu}{p}\right)} - 2\frac{p^2}{p_0^2}\left(1-\frac{i\nu}{p}\right)\right\}\left(\frac{1}{1-n^2}\right) + \left\{\frac{p^2}{p_0^2}\left(1-\frac{i\nu}{p}\right)\right\}^2 - \frac{\gamma_T^2 \frac{p^2}{p_0^2}\left(1-\frac{i\nu}{p}\right)}{1-\frac{p^2}{p_0^2}\left(1-\frac{i\nu}{p}\right)} - \gamma_L^2 = 0$$

This equation has for its solution the well known Appleton-Hartree expression for the refractive index

$$n^2 = 1 - \frac{2}{2\frac{p^2}{p_0^2}\left(1-\frac{i\nu}{p}\right) - \frac{\gamma_T^2}{1-\frac{p^2}{p_0^2}\left(1-\frac{i\nu}{p}\right)} \mp \sqrt{\frac{\gamma_T^4}{\left(1-\frac{p^2}{p_0^2}\left(1-\frac{i\nu}{p}\right)\right)^2} + 4\gamma_L^2}} \qquad (12)$$

The refractive index is four valued, the solutions of equation (12) corresponding to the up-going ordinary wave, the up-going extraordinary wave, the down-coming ordinary wave and the down-coming extraordinary wave. The complex polarisation of plane waves advancing along the z axis is defined by the ratio of the complex components of the field in the XY plane. Using equations (4) and (10) we obtain

$$R = \frac{E_y}{E_x} = -\frac{H_x}{H_y} = \frac{P_y}{P_x} = \frac{i}{\gamma_L}\left(\frac{1}{1-n^2} - \frac{p^2}{p_0^2}\left(1-\frac{i\nu}{p}\right)\right) \qquad (13)$$

Reflection of an up-going wave is considered to occur at the electron density level for which the appropriate value of the refractive index is zero for zero collision frequency, or approaches zero when the collision frequency is small ($\frac{\nu}{p} \ll 1$). In general, for all conditions of wave frequency and geomagnetic field, only three such levels of reflection are found. The refractive index equation may be used to discuss the circumstances in which reflection at these levels occur, although, because it is limited to slowly varying media, it does not describe the actual process of reflection.

2.3 Reflection Conditions.

At vertical incidence the direction of wave propagation remains vertical and the propagation angle Θ will equal the inclination of the geomagnetic field to the vertical at all levels. It is necessary, therefore, only to consider how the refractive index changes with electron density and collision frequency.

(i) Collision frequency zero.

(a) Quasi-transverse propagation (non vertical magnetic field)

$$\frac{\pi}{2} \geqslant \Theta > 0$$

$$n^2 = 1 - \frac{p_0^2}{p^2 - \frac{p_H^2 \sin^2\theta}{2\left(1 - \frac{p_0^2}{p^2}\right)} \mp \sqrt{\frac{p_H^4 \sin^4\theta}{4\left(1 - \frac{p_0^2}{p^2}\right)^2} + p^2 p_H^2 \cos^2\theta}} \qquad (14)$$

The reflection levels($n = o$) are given by:

		polarisation of emergent wave.
1.	$\frac{p_0^2}{p^2} = 1 - \frac{p_H}{p}$	Left handed.
2.	$\frac{p_0^2}{p^2} = 1$	Right handed.
3.	$\frac{p_0^2}{p^2} = 1 + \frac{p_H}{p}$	Left handed.

The corresponding angular critical frequencies are:

1. $p_c = \sqrt{p_0^2 + \frac{p_H^2}{4}} + \frac{p_H}{2}$
2. $p_c = p_0$
3. $p_c = \sqrt{p_0^2 + \frac{p_H^2}{4}} - \frac{p_H}{2}$

The polarisation of the down-coming emergent waves is left-handed elliptical for the wave reflected at level 1 and right-handed for the one reflected at level 2. Reflection at levels 1 and 2 has long been identified with the observed double splitting of echoes into extraordinary and ordinary components respectively. The anomalous Z echo then has the properties of critical frequency and height of reflection consistent with reflection at the third level, that is:

$$N_3 > N_2 > N_1$$

$$p_{c2} - p_{c3} \sim \frac{p_H}{2} \qquad p >> p_H$$

$$p_{c1} - p_{c3} = p_H$$

The three levels of reflection will hereafter be referred to as the X, O and Z levels respectively.

(b) <u>Lòngitudinal Propagation</u>

If the magnetic field is vertical, ($\theta = 0$) we have:

$$n^2 = 1 - \frac{p_0^2}{p^2 - \frac{p_H^2}{2\left(1 - \frac{p_0^2}{p^2}\right)} \mp \frac{p_H^2}{2\left(1 - \frac{p_0^2}{p^2}\right)}} \qquad (15)$$

Here, n = 0 when polarisation

$$\frac{p_0^2}{p^2} = 1 - \frac{p_H}{p} \qquad \text{Left Handed}$$

$$\frac{p_0^2}{p^2} = 1 + \frac{p_H}{p} \qquad \text{Right Handed}$$

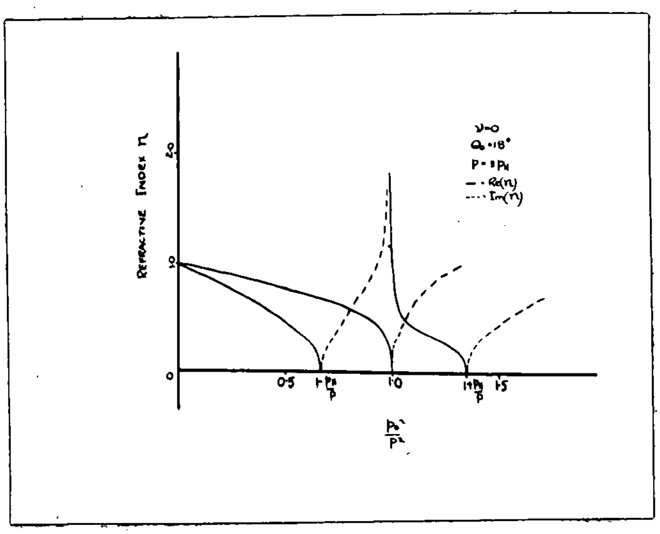

FIG. 3

Variation of Refractive Index with $\frac{p_0^2}{p^2}$ for the case of Quasi-transverse Propagation.

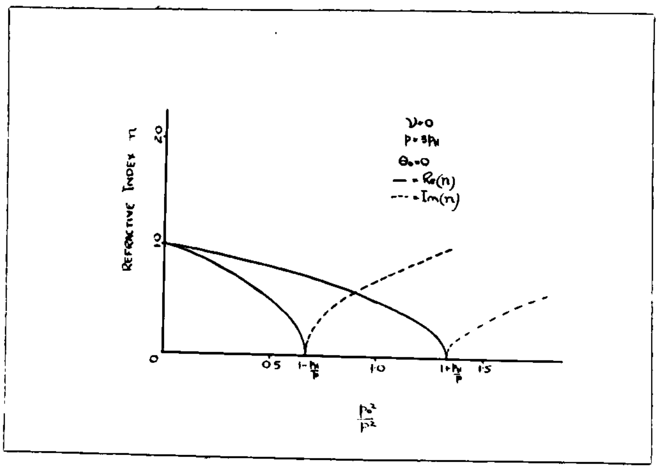

FIG. 4

Variation of Refractive Index with $\frac{p_0^2}{p^2}$ for the case of Longitudinal Propagation.

(ii) <u>Effect of Collisions.</u>

If a small but finite collision frequency ($\frac{\nu}{p} \ll 1$) is used in the Appleton-Hartree formula the zeroes and infinities of the refractive index disappear and also the transition between the quasi-transverse and longitudinal types of propagation occurs not at $\Theta = 0$ but when the propagation angle is related to the collision frequency according to the expression

$$\nu = \frac{p_H \sin^2\Theta}{2\cos\Theta} \qquad (16)$$

If the propagation angle is considered to be constant it is usual to refer to the corresponding value of ν as the critical collision frequency ν_c. Conversely, if ν is given we have the critical propagation angle at which the transition occurs Θ_c.

It can be seen from Fig.5 that, using collisions, real refractive index paths up to all three reflection levels can be found in the case of quasi-transverse (Q.T.) propagation. However, reflection at the Z level can occur only after the X wave has penetrated the region between the X and Z levels where the imaginary part of the refractive index, and therefore the attenuation, is high.

The refractive index curves for quasi-longitudinal propagation are essentially the same as in the collision-free case, that is, reflection can only occur at the X and Z levels.

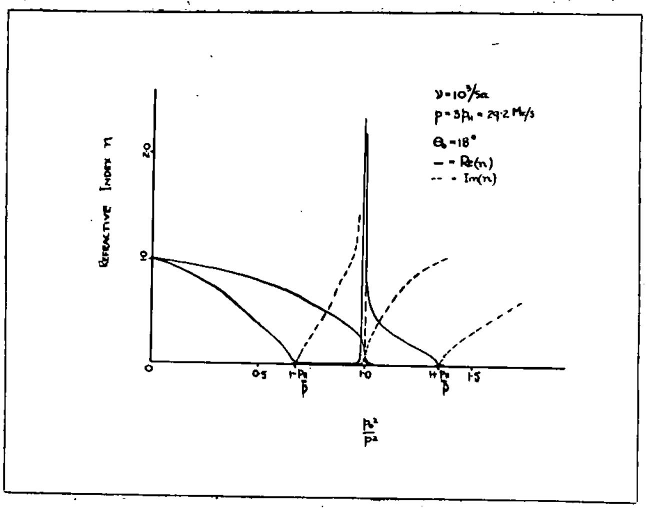

FIG. 5.

Variation of Refractive Index with $\frac{p_0^2}{p^2}$ for the case of Quasi-transverse Propagation (small collision frequency)

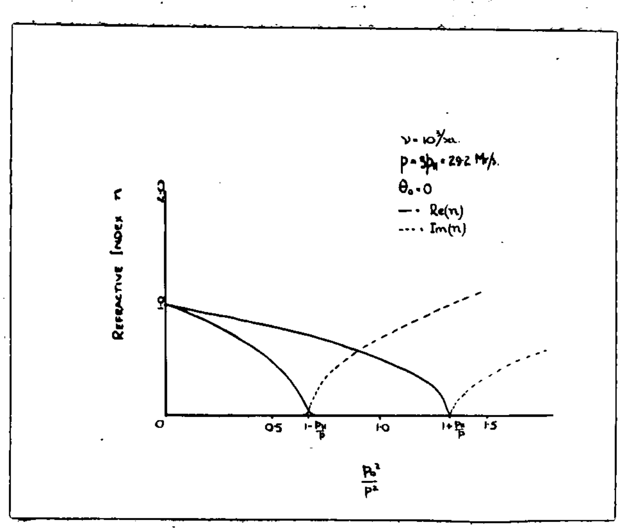

FIG. 6

Variation of Refractive Index with $\frac{p_0^2}{p^2}$ for the case of Quasi-longitudinal Propagation (small collision frequency)

The estimated values of collision frequency in the ionosphere are such that Q.L. propagation can occur in the F region at vertical incidence only in the immediate vicinity of the earth's magnetic poles. For example, Fig.7 shows a curve of variation of collision frequency with height, published by Gerson (13). From this we obtain the curve shown in Fig.8 for the inclination of the earth's magnetic field necessary at different heights for Q.L. propagation. We see that in the F region above 200 Km. Q.L. propagation will occur only at places where the magnetic field is closer than 2.6° to the vertical.

According to the vertical incident Appleton-Hartree ray theory, therefore, the only way in which simultaneous reflection at all three possible levels can occur at medium magnetic latitudes is through the Q.T. propagation of the X wave up to the Z level. This mechanism was first proposed by Mary Taylor (14). It would produce extraordinarily polarised Z echoes and could, therefore, be tested experimentally by polarisation methods.

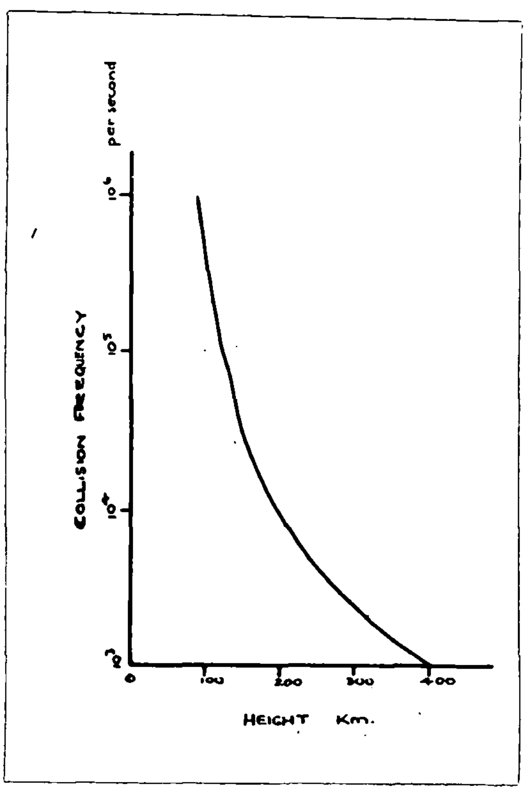

FIG. 7

Variation of Estimated Collision Frequency with Height.

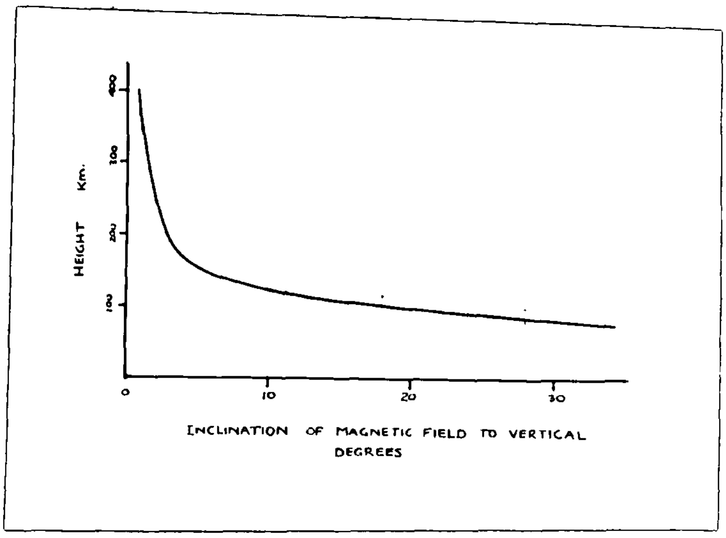

FIG . 8,

Inclination of the Magnetic Field at which the Q.L. - Q.T.

Transition Occurs.

2.4 The Coupling Theory of Triple Splitting.

On physical grounds one might expect a continuous transition from Q.T. to Q.L. propagation with reflection at all three levels when $\Theta = \Theta_c$. The third echo in this case would be ordinarily polarised and would correspond to Q.L. reflection at the Z level. It was suggested by Eckersley (15) in 1950 that the transition may take place relatively slowly with change in Θ , allowing partial Q.L. reflection at the Z level, even at places where $\Theta >> \Theta_c$. This idea was placed on a quantitative basis by Rydbeck (8) who obtained approximate solutions to the wave equations (8a) and (8b). Rydbeck developed these solutions to the point where the probability of Q.L. propagation to the Z level could be estimated for any value of the propagation angle and of the collision frequency.

Rydbeck's method consists essentially of reducing the four propagation equations to two coupled differential equations by separating the field components into ordinary and extraordinary parts. Under certain circumstances, which are discussed below, approximate solutions may then be obtained to these two coupled equations. The process of reduction depends on the recognition that in equation (8a) the ratios

$\frac{E_x}{P_x}$ and $\frac{E_y}{P_y}$ become identical for a certain value of the polarisation ratio $\frac{P_y}{P_x}$ and thus they belong to the same wave solution.

This condition $\frac{E_x}{P_x} = \frac{E_y}{P_y}$ may therefore be used to define the two principal modes of propagation, having the polarisations

$$\frac{E_{y_1}}{E_{x_1}} = u_1 \qquad\qquad \frac{E_{y_2}}{E_{x_2}} = u_2$$

where u_1 and u_2 are obtained from equation (13), that is:

$$u_{1,2} = \frac{i}{1-\frac{p_0^2}{p^2}}\left[\frac{p_H \sin^2\theta}{2p\cos\theta} \mp \sqrt{\frac{p_H^2 \sin^4\theta}{4p^2\cos^2\theta} + \left(1-\frac{p_0^2}{p^2}+\frac{i\nu}{p}\right)^2}\,\right] \qquad (17)$$

Using these relations between E_{x_1}, E_{y_1}, E_{x_2}, E_{y_2} in equation (8a) it may be easily shown that

$$D_{y_1} = n_1^2 E_{y_1}, \quad D_{y_2} = n_2^2 E_{y_2}, \quad D_{x_1} = n_1^2 E_{x_1}, \quad D_{x_2} = n_2^2 E_{x_2}$$

Also, using the relations

$$D_x = D_{x_1} + D_{x_2} \qquad\qquad D_y = D_{y_1} + D_{y_2}$$

and by forming new field components Π_1, Π_2 according to the transformations

$$\Pi_1 = \frac{E_{x_1}}{\sqrt{1-u_1^2}} \qquad\qquad \Pi_2 = \frac{E_{y_2}}{\sqrt{1-u_2^2}} \qquad (18)$$

then equations (8a) and (8b) finally may be reduced to the following two coupled wave equations

$$\frac{\partial^2 \Pi_1}{\partial z^2} + \left(\frac{p^2 n_1^2}{c^2} + M^2\right)\Pi_1 = -\Pi_2 \frac{\partial M}{\partial z} - 2\frac{\partial \Pi_2}{\partial z}.M$$

$$\frac{\partial^2 \Pi_2}{\partial z^2} + \left(\frac{p^2 n_2^2}{c^2} + M^2\right)\Pi_2 = -\Pi_1 \frac{\partial M}{\partial z} - 2\frac{\partial \Pi_1}{\partial z}.M \qquad (19)$$

where $\quad M = \left(\frac{1}{1-u^2}\right)\frac{\partial u}{\partial z}$

M is termed the coupling coefficient since, when M is negligible, equations (19) become uncoupled and separate O and X solutions can be obtained. This is the case over all but local regions of the ionosphere and, except in these coupling regions, there is essentially independent propagation of the ordinary and extraordinary modes. We may obtain approximate solutions to these equations of the well known W.K.B. type

$$\Pi = \left(\frac{pn}{c}\right)^{-\frac{1}{2}}\left(A e^{-i\int \frac{pn}{c} dz} + B e^{i\int \frac{pn}{c} dz}\right) \qquad (20)$$

providing several conditions are satisfied. It is necessary that the coupling coefficient be small, that is $M^2 \ll \frac{pn^2}{c^2}$ and the right-hand side of the equation is allowed to have only a negligible effect; also we need $\frac{\partial n}{\partial z} \ll n^2$ the condition for a slowly varying medium.

The first term in the solution represents an up-going wave travelling in the Z direction. In the neighbourhood of a reflection point the approximate solution breaks down and the up-going wave is transformed into a down-coming wave represented by the second term

Since the refractive index is four valued it may be represented as a single valued function on a four sheeted Riemann surface, using the height as a complex co-ordinate $z = u + iv$ Branch points connecting the up-going and down-coming sheets are defined by $n(z) = 0$ or by $n(z) = \infty$. Coupling points which connect ordinary and extraordinary sheets are defined by $n_1 = n_2$. The polarisation vector $u = \mp 1$ at these points and consequently the coupling coefficient becomes infinite. Fig.9 shows the location of the branch points in the Riemann surface. The reflection points are given by

$$\frac{p_0^2}{p^2} = 1 - \frac{i\nu}{p} \quad \text{and} \quad \frac{p_0^2}{p^2} = 1 \mp \frac{p_H}{p} - \frac{i\nu}{p} \qquad (21)$$

and the coupling points by

$$\frac{p_0^2}{p^2} = 1 - \frac{i\nu}{p} \mp \frac{i\nu_c}{p} \qquad (22)$$

Since the W.K.B. approximation is restricted to a slowly varying medium, it obviously cannot be used in the neighbourhood of a branch point. But if it is possible to find a good path around the branch point, such that the condition $\frac{\partial n}{\partial z} \ll n^2$ is fulfilled, the solution is useful and the transmission coefficient can be expressed by

$$T = e^{-\int \frac{p}{c} n \, dz}$$

If the existence of any good path can be taken for granted it is convenient for calculations to use a path right over the branch point.

In the case of Q.L. propagation to the Z level, we are interested in the transmission coefficient of the ordinary wave through the Q.T. ordinary level of reflection. The integration is carried out along the line

$$\frac{p_0^2}{p^2} = 1 - \frac{i\nu}{p} + \frac{i\nu_c\lambda}{p} \qquad \text{where } \lambda = \frac{\nu}{\nu_c}$$

which joins the coupling points. At the ordinary reflection point we have $\lambda = 0$ and at the coupling points $\lambda = \mp 1$. Along this line for which $Re\left(\frac{p_0^2}{p^2}\right) = 1$ we may write the Appleton-Hartree formula

$$n^2 = \frac{1 \mp \sqrt{1-\lambda^2} + \frac{\lambda^2 \nu_c}{p_L}}{1 \mp \sqrt{1-\lambda^2} + \lambda\left(i - \frac{\nu}{p}\right)\frac{p}{p_L}} \qquad (24)$$

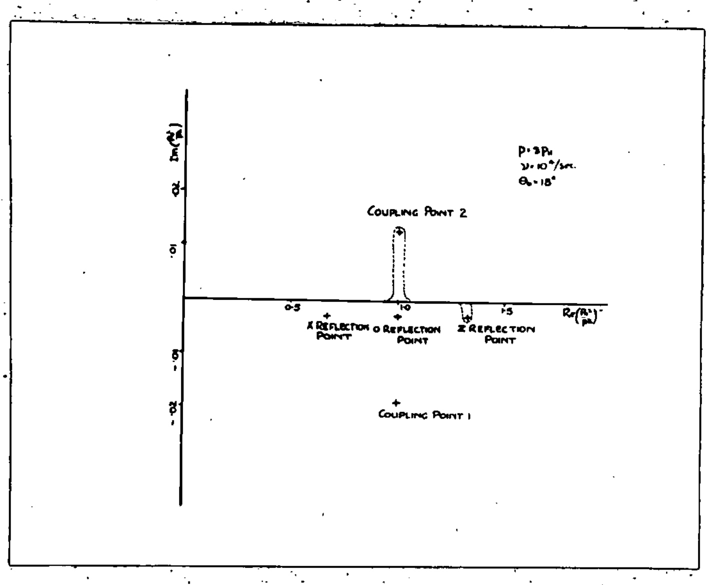

FIG. 9.

Branch Points and Integration Path in the Complex Plane.

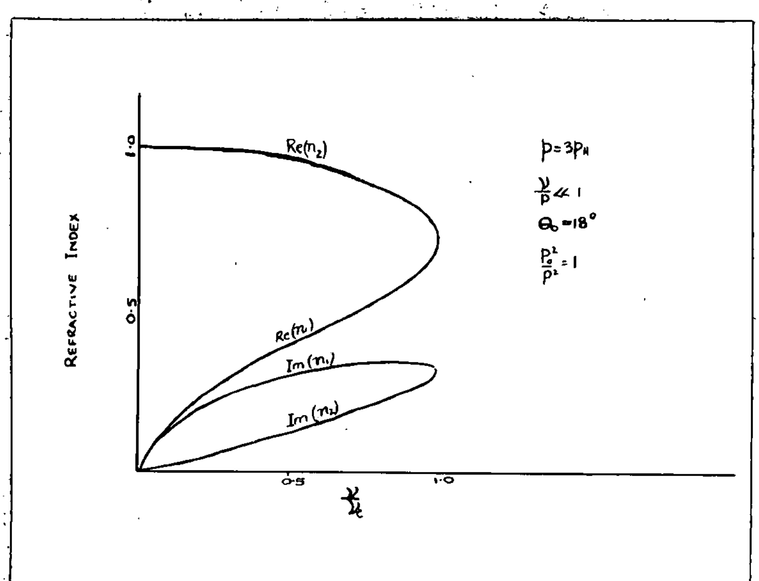

FIG. 10.

Variation of Refractive Index along the Line joining the Coupling Points.

The integration is carried out between the real axis and the nearer coupling point (2). Since in Fig.10 the real axis occurs at $\lambda = \frac{\nu}{\nu_k}$ it is obvious that as $\nu \to \nu_k$ the position of the coupling point will approach the real axis until when $\nu = \nu_k$ the integration path remains on the real axis through the coupling level. The coefficient of transmission of ordinary waves through the coupling level will then become unity. There will thus be a continuous transition from Q.T. reflection at the ordinary or coupling level to Q.L. reflection at the Z level with reflection at both levels over a certain range of values of ν or Θ

Although Rydbeck advanced the coupling theory as an explanation of triple splitting, he did not consider in detail the application of the theory, using typical F region values of collision frequency. When this is done it is found that the predictions of the coupling theory do not differ essentially from those of the Appleton-Hartree ray theory except at places where the magnetic field is very nearly vertical. For example, Fig.11 shows the results of calculations of the power transmission coefficient of propagation of O waves twice through the coupling level for different conditions of magnetic field and collision frequency. The attenuation according to the Appleton-Hartree theory is also shown.

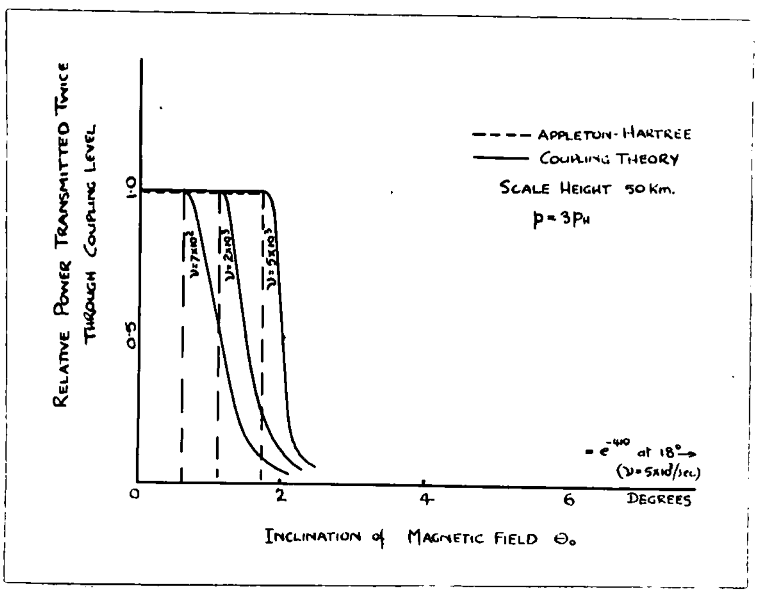

FIG.11

Transmission of O Waves through the Coupling Level.

It is obvious that the coupling theory, instead of providing an explanation of vertical incidence triple splitting in the F region at middle latitudes, actually demonstrates the reverse, that is, it is most unlikely that triple splitting is due to Q.L. penetration of the O wave through the coupling level. However, as we have seen, such a mechanism would produce ordinarily polarised Z echoes and could therefore be tested by polarisation methods.

2.5 Oblique Incidence Triple Splitting.

In 1950 Scott (6) and Dieminger (16) independently proposed that ordinarily polarised Z echoes may be due to oblique back-scattering of part of the incident wave. Scott suggested that longitudinal propagation may occur along the direction of the geomagnetic field with Z echo reflection by ionospheric irregularities near the magnetic zenith of the observer. This idea was not worked out in any detail, although observations by Dieminger indicated that F region triple splitting was associated with the occurrence of spread F echoes, that is, with disturbed ionospheric conditions under which oblique back-scattering from ionospheric irregularities might be expected.

2.6 Summary.

It has been the intention in this review to describe the position of triple splitting theory as it was in 1951 when this investigation was begun. As we have seen, Rydbeck's was the only theory which has been considered in detail and this gave a negative result. The other possibilities of the Q.T. X wave Z echoes of Mary Taylor and of the oblique back-scattered echoes of Scott could not be assessed at the time and it was felt that the most convincing way of arriving at the correct explanation would be to obtain additional unambiguous experimental evidence of Z echo characteristics. The properties which Z echoes might be expected to have, according to the three alternative explanations, are summarised below:

	Type of Propagation	Polarisation	Direction of Arrival
Mary Taylor	Quasi-transverse	X	Vertical
Eckersley and Rydbeck	Quasi-longitudinal	O	Vertical
Scott and Dieminger	Oblique	O	18°

It is clear that knowledge of the sense of polarisation and of the direction of arrival of Z echoes would lead to definite conclusions regarding the actual mechanism of F region triple splitting. The results of measurements of these quantities, which were made at Hobart, are discussed in the next section.

3. POLARISATION AND ANGLE OF ARRIVAL MEASUREMENTS.

3.1 The Polarisation of Z echoes.

Polarisation measurements, using the circular polarisation receiver described in Section 7.1, were begun in August 1951. The polarisation sense of all echoes was recorded automatically once hourly on a frequency of 3.3 Mc/s. Observations were synchronised with a P'f recorder which was used to identify the Z echoes. For the two months from August to October 1951 Z echoes were recorded on four occasions. In all cases the polarisation was approximately circular in a right-handed sense, that is, the echoes were ordinarily polarised. Fig.12 shows a typical photograph of the echo polarisations and Fig.13 a tracing of this record superimposed at the operating frequency on the simultaneous P'f record. At about the same time this result was confirmed by polarisation measurements on Z echoes made independently by Hogarth (17) in Canada and Landmark (18) in Norway.

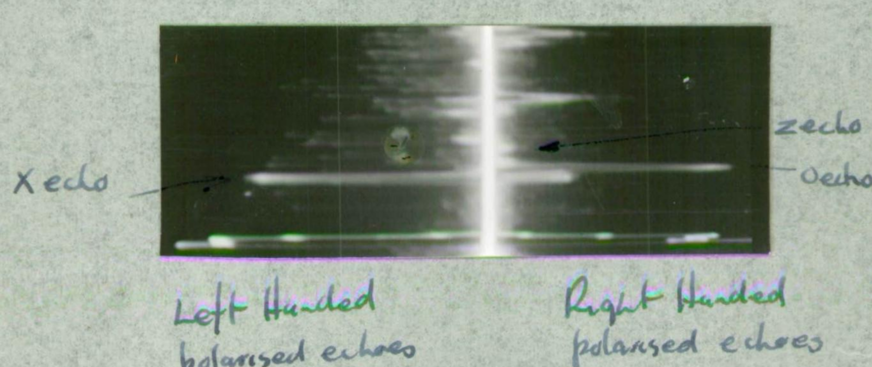

Hobart.
20-8-51
2000 hours.

FIG. 12

Polarisation Record showing the presence of a Z Echo.

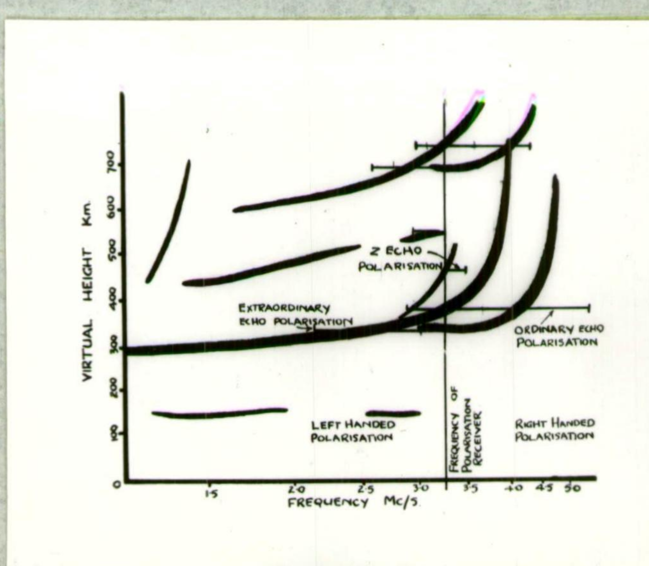

FIG.13 Tracing of Fig.12 superimposed on Simultaneous P'f Records.

3.2. The Angle of Arrival of Z Echoes.

To determine whether the ordinarily polarised Z echoes were due to vertical or oblique incidence propagation, direction finding measurements were begun in July 1952. The technique used was the well known one of observing the phase difference between the signals induced in two spaced loop aerials by a selected down-coming echo. (Ross et al (19)). The signals were amplified by a twin channel cathode ray D.F. receiver which is described in Section 7.2, together with associated equipment and the actual observational technique.

The quantities measured were the vertical angle of arrival Φ_i in the plane containing the geomagnetic field, and the vertical angle of arrival Ψ_i in the E-W plane. The results are summarised in Table 2. The direction of arrival of Z echoes was observed to vary in a random manner over a range of a few degrees with mean directions of 8.7°N. and 0.2°E. of the vertical. The E-W direction was not significantly different from zero.

It is apparent that F region Z echoes are due to oblique incidence backscatter from ionospheric irregularities, although the angle of incidence is considerably less than was expected.

TABLE 2.

Date	Time	No. of Observations.	Average Directions $\bar{\Phi}_i$ Degrees N.	$\bar{\Psi}_i$ Degrees	Deviations from Mean. $\lvert\Phi_i-\bar{\Phi}_i\rvert$ Degrees	$\lvert\Psi_i-\bar{\Psi}_i\rvert$ Degrees
3-9-52	1540	18	9.05	.35 E.	.54	.48
10-9-52	1540	22	8.75	.1 E.	.47	.44
17-9-52	1530	19	9.0	.5 E.	.69	.36
18-9-52	1600	21	9.0	.2 E.	.74	.55
26-9-52	1535	20	8.6	.3 E.	.52	.4
1-10-52	1550	22	9.3	.15 W.	.7	.6
3-11-52	1750	102	8.65	-	.55	-
22-4-53	1730	21	8.9	-	.68	-
26-4-53	1710	28	9.1	-	.6	-
1-5-53	1700	21	8.4	-	.4	-
2-5-53	1716	114	8.55	-	.54	-
12-5-53	1600	31	8.5	-	.65	-
18-5-53	1615	73	8.95	-	.59	-
22-5-53	1603	150	8.6	-	.55	-
29-5-53	1600	20	8.25	-	.75	-
5-6-53	1615	38	9.2	-	.6	
Average			8.7	.2E	.56°	.47°

Wave frequency = 4.65 Mc/s

4. THE THEORY OF TRIPLE SPLITTING.

To determine the reason for the observed angle of arrival of Z echoes it is necessary to examine the conditions of oblique incidence propagation in the plane of the geomagnetic field. Although Booker (20) has developed an oblique incidence magneto-ionic theory, this is unsuitable for surveying propagation conditions over a wide range of angles of incidence, except in those cases where an analytical solution can be found, that is, E.W. propagation and N.S. propagation at the magnetic equator.

We, therefore, use a graphical method developed by Poeverlein (21). With this method any unusual features in oblique incidence propagation are obvious by inspection.

4.1 Poeverlein's Method.

For any region of uniform electron density we may draw a polar diagram of refractive index against propagation angle with respect to the geomagnetic field direction, using the Appleton-Hartree refractive index equation. Suppose the region has an upper and lower boundary and that an E.M. wave is incident on one boundary from outside at angle of incidence ϕ_i. The direction of the wave normal in the region may then be determined as follows:

The polar diagram, which is analogous to the refractive index ellipsoid of crystal optics, is orientated centrally on a rectangular co-ordinate system OX, OY, OZ in which the plane y = o is parallel to the medium boundary. The plane z = o contains the magnetic field direction. A line drawn through the diagram parallel to the OY axis and distance $\sin\phi_i$ from the origin will intersect the refractive index surface in at least two points. The direction of the lines joining these points to the origin give the directions of the wave normal within the medium for an angle of incidence ϕ_i (See Fig.(14)). The two directions found in general correspond to waves incident on opposite boundaries. This result is obtained simply from Snell's law:

$$n \sin\phi_r = \sin\phi_i \qquad \phi_r = \text{angle of refraction}$$

It may also be shown that the direction of energy flow in the medium is given by the normal to the surface at the point of intersection.

In the case of an absorptive medium (using collisions) the diagram is drawn using the real part of the refractive index. The imaginary part of the refractive index at the point of intersection then gives the attenuation of a wave proceeding in the direction of a wave normal. When the medium is non-uniform and horizontally stratified, the direction of the wave normal at any level may be obtained from the intersection of the angle of incidence ordinate, with the refractive index surface for the appropriate level. If we define a reflection level by horizontal direction of energy propagation, then this level is given by the surface which is tangent to the ordinate. Figs. (15) and (16) show families of curves for the O and X waves for propagation in the vertical plane containing the geomagnetic field.

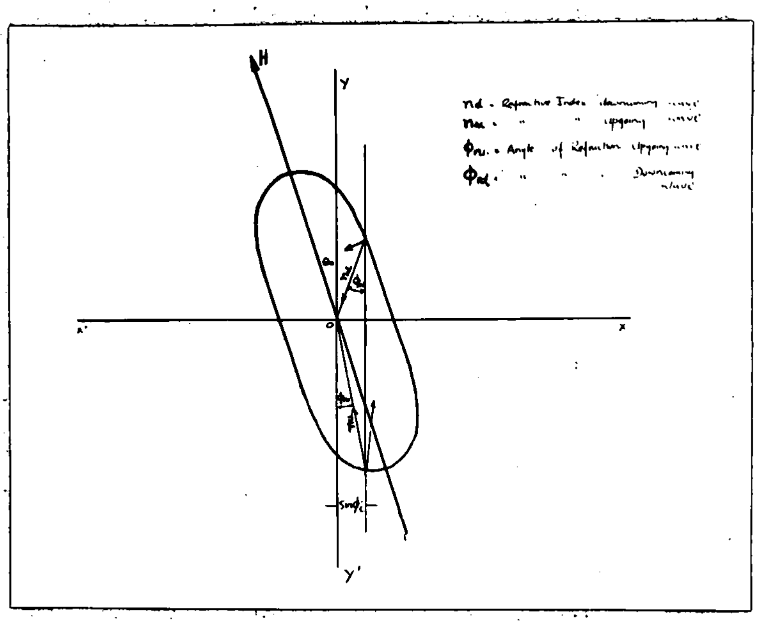

FIG.14. Section of the Poeverlein Diagram in the Plane of the Magnetic Field.

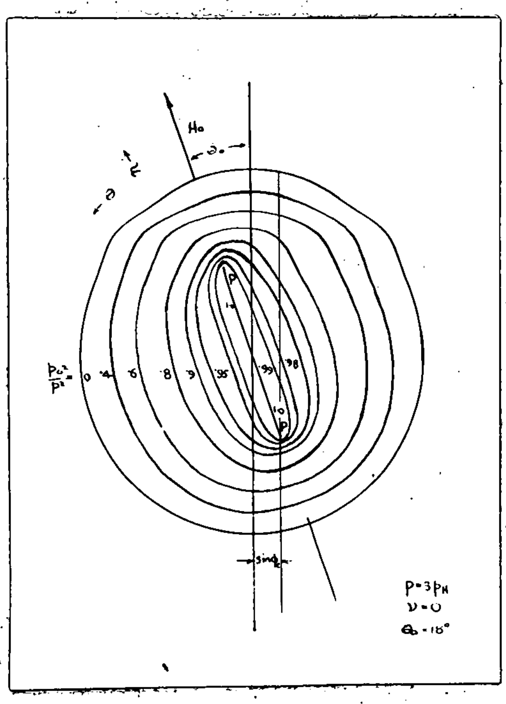

FIG.15. Refractive Index Polar Diagram, O-wave. Collision Frequency.Zero.

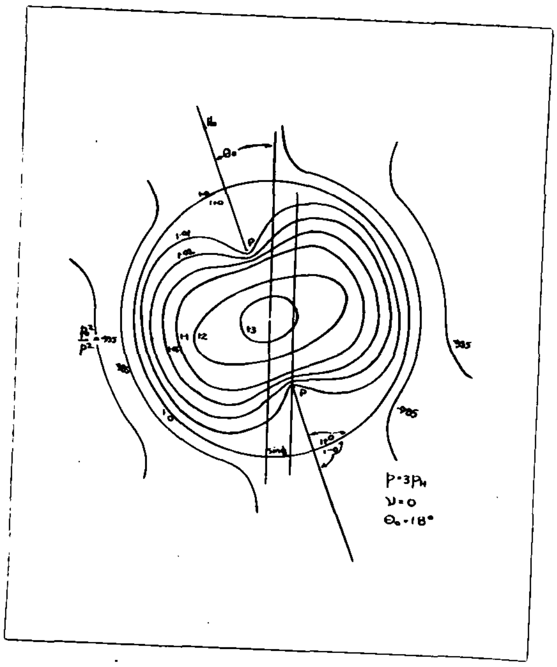

FIG. 16

Refractive Index Polar Diagram. X-wave. Collision Frequency Zero.

4.2 Application to Triple Splitting.

It is obvious from these diagrams that unusual propagation of an up-going ordinary wave may occur when the angle of incidence is given by the x co-ordinate of point P, which is common to both the O and X families of curves. For this angle of incidence the refractive index and direction of wave normal of the ordinary wave just below the level $\frac{p_0^2}{p^2} = 1$ will be very nearly the same as those of the X wave just above this level. Since both the O curves for $\frac{p_0^2}{p^2} < 1$ and the X curves for $\frac{p_0^2}{p^2} > 1$ are obtained from the same solution of the Appleton-Hartree equation (negative sign before the square root) the wave polarisations will also be the same. These features suggest that an up-going ordinary wave with this angle of incidence will pass through the normal level of reflection at $\frac{p_0^2}{p^2} = 1$ and continue on until reflected at the higher level near $\frac{p_0^2}{p^2} = 1 + \frac{p_H}{p}$. On its downward path the wave will run into an infinite refractive index barrier slightly below the $\frac{p_0^2}{p^2} = 1$ level. If scattering occurs during the process of reflection sufficient energy may be scattered back along the incident path to produce observable oblique incidence Z echoes. The refractive index paths for angles of incidence near the critical angle may be illustrated by plotting Booker's q = $n \cos \phi_r$

as a function of electron density. These curves are shown in Figs.17,18,19. The critical angle of incidence is obtained from the co-ordinates of a point P, that is:

$$\sin \phi_c = \sqrt{\frac{q}{1+q}} \sin \Theta_c \qquad (25)$$

where

$$q = \frac{p_H}{p}$$

After arriving at this explanation of oblique incidence Z echoes it was discovered that Poverlein had also suggested that an O wave might be propagated through the O level of reflection when the angle of incidence is given by Equation (25). However, he apparently did not consider the possibility of the back-scattering of such a wave.

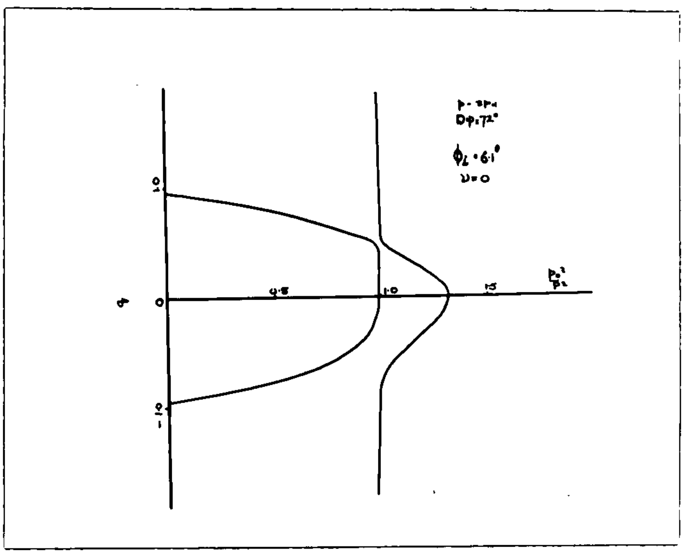

FIG. 17

Variation of q with $\frac{p_o^2}{p^2}$ when $\phi_i < \phi_c$

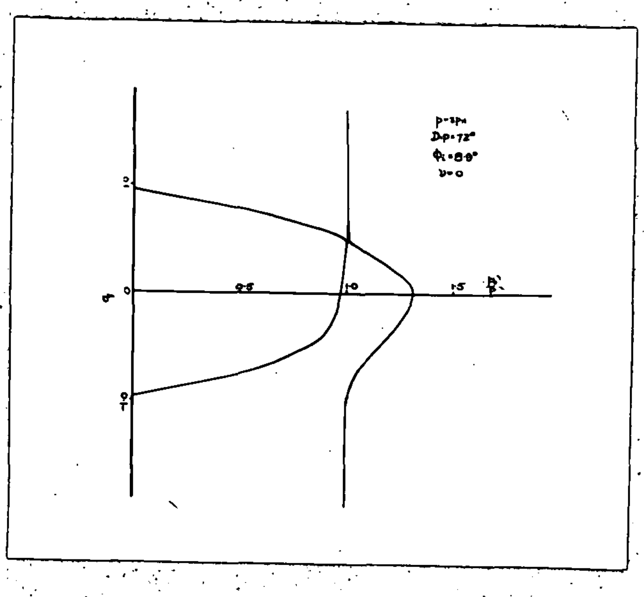

FIG . 18

Variation of q with $\frac{p_o^2}{p^2}$ when $\phi_i = \phi_c$

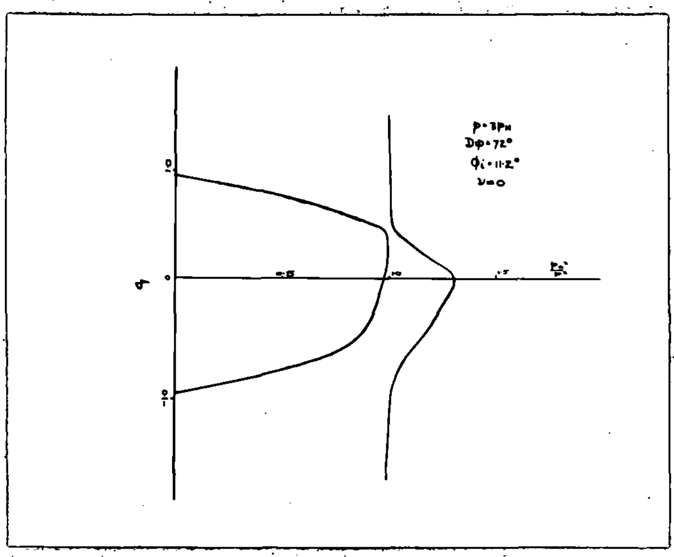

FIG. 19

Variation of q with $\frac{p_o^2}{p^2}$ when $\phi_i > \phi_c$

4.3 Comparison with Experiment.

The critical angle of incidence equals almost exactly the observed angle of arrival of Z echoes. Fig.20 shows curves of Φ_c for different frequencies and values of magnetic dip, together with the observed angles of arrival. That the agreement is not accidental was shown by independent angle measurements of Z echoes made in Germany by Moller (22) under different conditions of frequency and magnetic field. His results are also given in Fig.20.

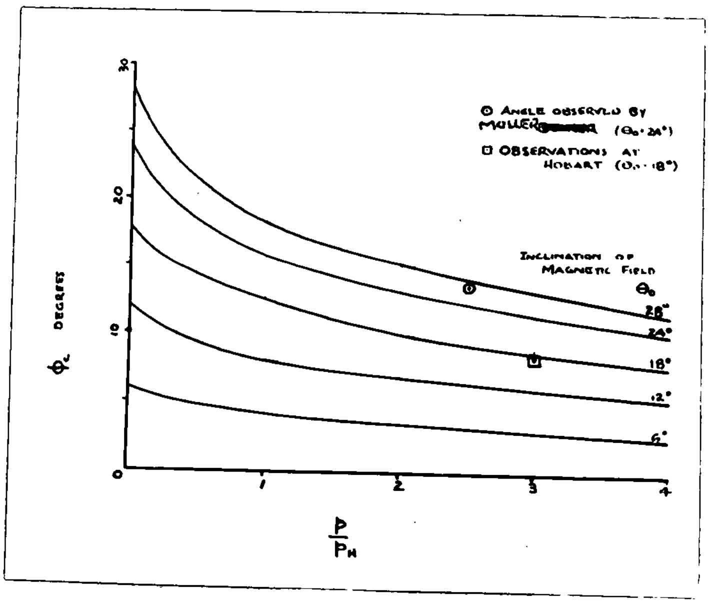

$f_H = 1.55$ Mc/s Hobart (at 200Km)

FIG. 20

Variation of the critical angle of incidence with frequency and magnetic dip.

These results thus afford an experimental demonstration that F region Z echoes are due to backscattered O waves which have penetrated the O level of reflection at oblique incidence.

4.4 Effect of Collisions.

In the case of vertical incidence propagation the introduction of collisions increases from zero the propagation angle for which quasi-longitudinal penetration of the O level can occur. It is of interest to see whether an analogous situation exists near the critical angle of oblique incidence. At vertical incidence a useful criterion for quasi-longitudinal propagation is that the refractive index curve of the O wave is continuous through the O level and up to the Z level. For quasi-transverse propagation a discontinuity exists at the O level. By analogy one might expect that for a range of angles of incidence near ϕ_c, O wave refractive index paths continuous through the O level might be obtained.

The refractive index polar diagrams using a typical value of collision frequency in the F region are shown in Figs, 21 and 22. Here points P_1 and P_2 are the coupling points at which the complex O and X refractive indices are equal for $\frac{p_c^2}{p^2} = 1$. They occur at the Q.T. to Q.L. transition propagation angle. The curves for $\frac{p_c^2}{p^2} \sim 1$ are markedly different from the collision-free case. For $\left|1 - \frac{p_c^2}{p^2}\right| > .01$ in the case treated the difference becomes negligible.

The simplicity of the Poeverlein diagrams disappears when collisions are included and q curves plotted from them show a number of unusual features. For angles of incidence between zero and ϕ_c the up-going O wave curve does not connect simply at the O level with the down-coming O curve, but instead joins the X curve which eventually reaches the Z level of reflection. When $\phi = \phi_c$ the O wave curve is continuous and straight through the O reflection level. Since Z echoes come mainly from the direction ϕ_c it is apparent that the continuity of the O curve up to the Z level is mis-leading at other angles of incidence.

It is obvious that the analysis breaks down completely in the vicinity of the ordinary reflection level where the medium is not even approximately slowly varying and large changes in refractive index occur within very small fractions of a wave length. For even a qualitative theoretical treatment of the process by which the O wave penetrates the O level, it would be necessary to use an oblique incidence coupling theory. Since appropriate solutions of the oblique incidence wave equations are not yet available, any further information about this process must be derived from experimental observations . In section 5 we describe measurements which provide some information of the penetration process.

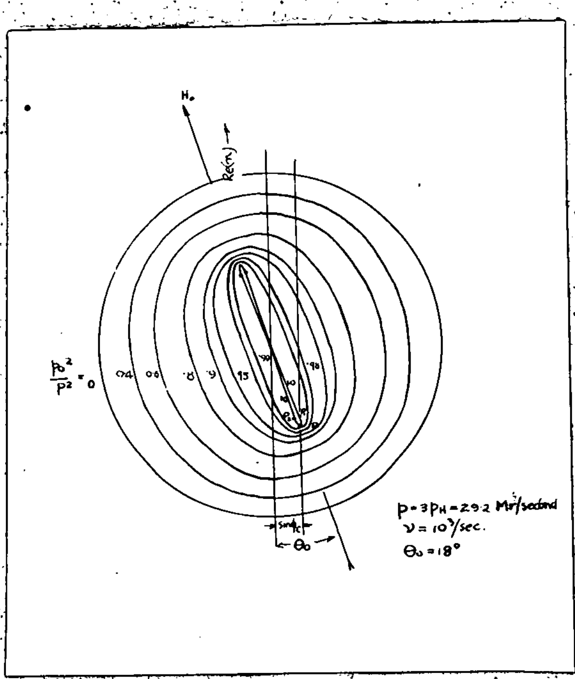

FIG. 21. Refractive Index Polar Diagram with small collision frequency. O-wave.

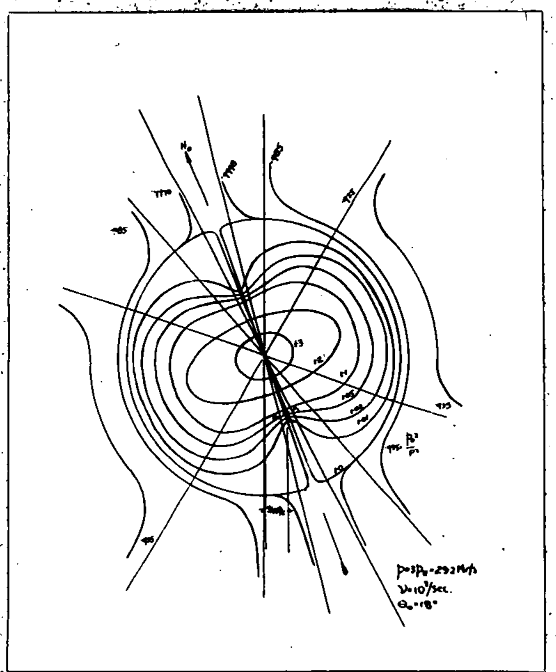

FIG. 22. Refractive Index Polar Diagram with small collision frequency. X-wave.

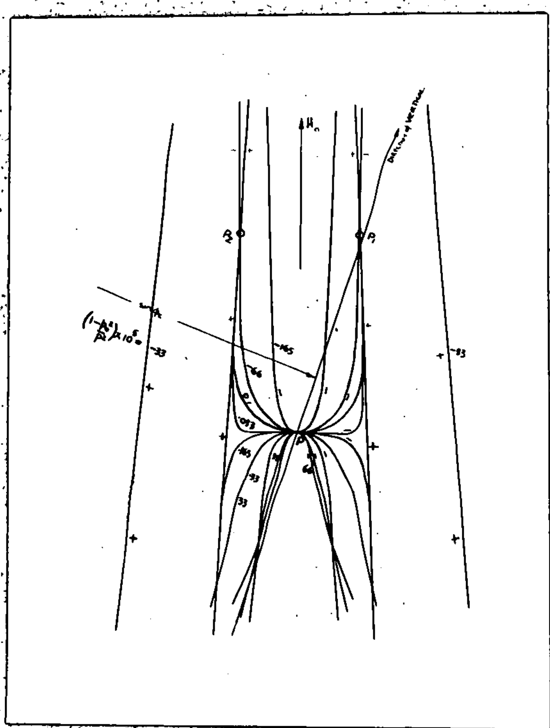

FIG.22 a. Enlargement of Fig. 22. in the vicinity of the coupling points P_1 and P_2.

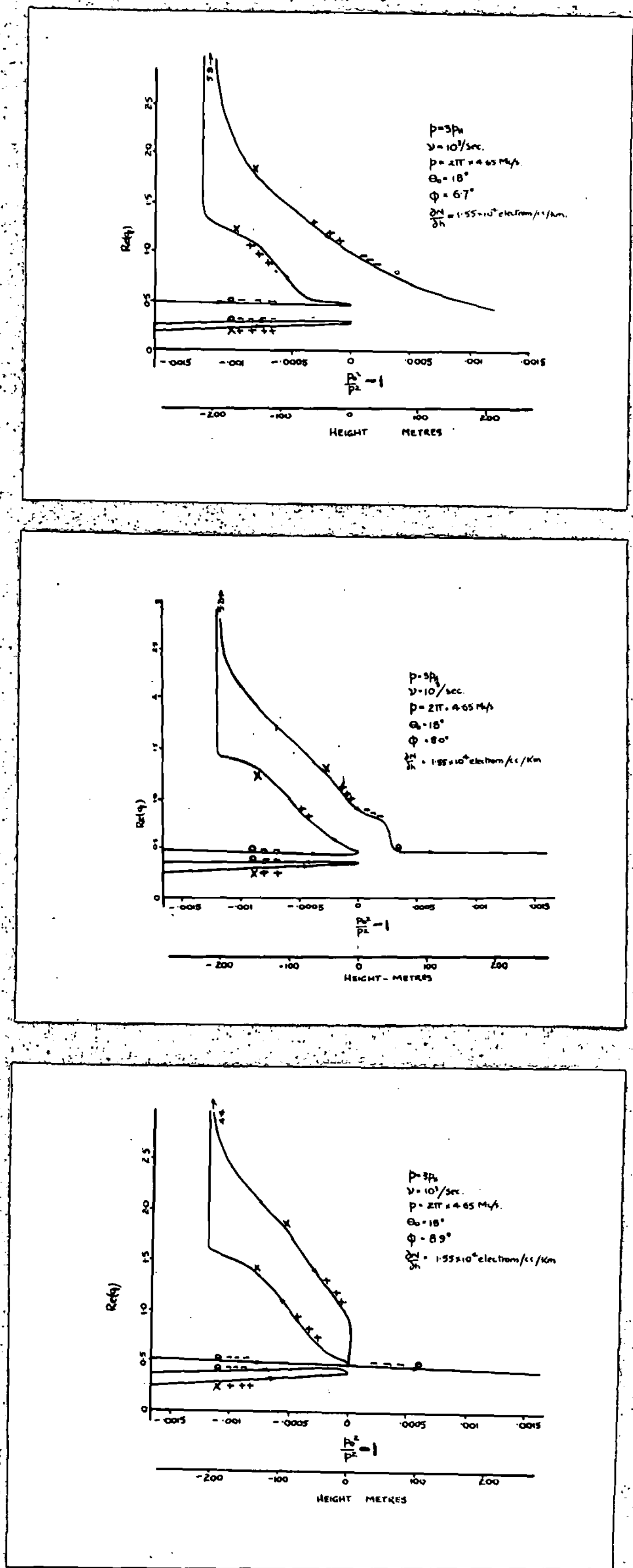

$\phi_i = \phi_c$

FIG. 23.

Showing the variation of q with $\frac{p_0^2}{p^2}$ for different angles of incidence between 0 & ϕ_c when the collision frequency $\nu = 10^3$/sec.

The plus and minus signs are those used in the A-H formula before the square root sign.

4.5 E. Region Triple Splitting.

In the E region the collision frequency is sufficiently high (See Figs.7 and 8) to allow quasi-longitudinal propagation at vertical incidence at medium magnetic latitudes. There are, however, certain features which require discussion. It was noticed by Meek (4), Rydbeck (8) and Scott (6) that the F_1 Z trace on P'f records shows evidence of group retardation at the frequency f_oE. This effect was considered by Rydbeck as evidence that E and lower F_1 Z echoes are produced by coupling in the E region. Suppose that between f_zE and f_oE, less than critical coupling occurs at the O level of reflection in the E region at vertical incidence. Part of the incident energy will be reflected as an O wave and part transmitted as a Z wave which will have the group retardation of the O wave up to the O level. The Z wave will penetrate the E layer maximum since the frequency is greater than f_zE. It will be observed after reflection as an F_1 Z echo. Near f_oE, this echo should show observable group retardation similar to that of the E layer ordinary echo on the same frequency. This phenomenon is illustrated by the P'f record of Fig.24 which shows in unusual detail the F_1 Z trace near f_oE. It can be seen that near this frequency the Z trace divides into stronger and weaker components, the former showing evidence of group retardation, while the latter does not. It seems likely, therefore, that in the E and lower F_1 regions, Z echoes are due both to vertical incidence coupling and to oblique incidence backscatter. No angle measurements were made on echoes of this type because they are generally very weak at Hobart.

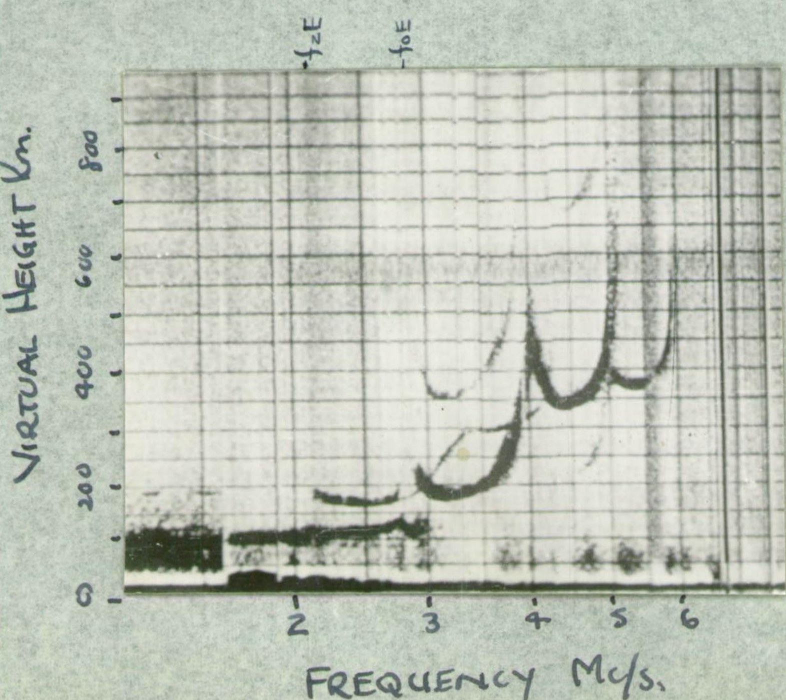

FIG. 24. P'f Record of 1020 hours; 22-12-50, Macquarie Is., showing split Z trace at f_oE.

Geographic Coordinates 54.5°S 160E
Geomagnetic Coordinates 61°S 243°E

5. THE ANGULAR POWER SPECTRUM OF Z ECHOES.

The distribution of Z echo power with angle of arrival will be determined by the angular attenuation function of the propagation hole together with any scattering of the waves which may occur between the ground and the level of the hole. Should an oblique incidence coupling theory become available, an experimental determination of the characteristics of the hole would be of some interest in checking the theory. However, it would first be necessary to demonstrate that lower level scattering is negligible. In the case of other applications of the propagation hole, to be discussed later, we are interested only in the angular power spectrum of the waves as they arrive at the ground.

There is a direct way of obtaining information about the angular power spectrum which is based on the unique property of Z echoes that they are returned to the ground in a narrow beam. If a receiver is moved in a horizontal direction away from the transmitter, then the area of the Z reflection level seen by the receiver will cease to coincide with that illuminated by the transmitter. As the distance is increased the Z echo power will decrease in a way which may be related to the form and parameters of the angular power spectrum. This property of Z echoes is due to the fact that the direction of the propagation hole is always relative to the observer.

The parameters of an assumed power spectrum may also be obtained from a statistical analysis of the random fluctuation in direction of arrival. This method, which has been treated by MacDonald (23) and Bramley (24), affords an independent way of checking measurements based on the beam effect of Z echoes.

5.1 The Theory of the Z Beam.

Suppose we have a rectangular co-ordinate system on the ground centred on the transmitter and orientated with the XOX^1 axis along the magnetic meridian. Let the co-ordinates of the receiver be (a,b) and let D be the projection of this point in direction ϕ_c north of the vertical on to a flat ionospheric layer. Points D and A, the projection of the origin in the same direction, represent the centres of the propagation hole with respect to the receiver and the transmitter.

We also use two angular co-ordinate systems based on the vertical and perpendicular planes through OA and BD.

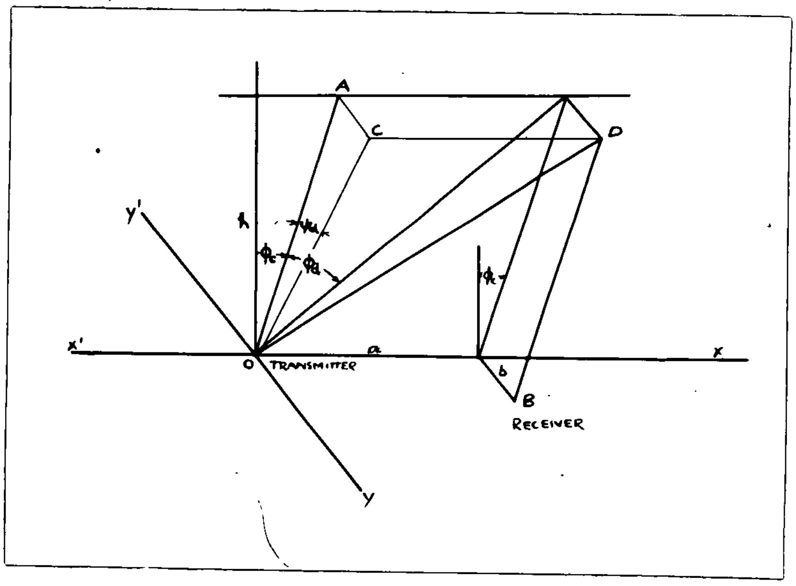

FIG. 25.

Co-ordinate System.

As we shall see, most of the power transmitted from O will pass through the propagation hole within a couple of degrees of OA. We may, therefore, write for the angular co-ordinates of D with respect to OA

$$\phi_d \sim \frac{a\cos^2\phi_c}{h} \qquad (26)$$

$$\psi_d \sim \frac{b\cos\phi_c}{h}$$

and if the angular co-ordinates of an element of area $dx\,dy$ of the reflecting layer with respect to OA are (ϕ,ψ) then its co-ordinates with respect to BD will be

$$(\phi-\phi_d \;,\; \psi-\psi_d)$$

Let the angular power spectrum of Z echoes at the transmitting point be

$$P(\phi,\psi) \qquad (27)$$

the power incident on an element of area of the reflecting level will then be represented by

$$\propto \sqrt{P(\phi,\psi)}\;\; d\phi\, d\psi \qquad (28)$$

and the power received at point B from this element by

$$\propto \sqrt{P(\phi,\psi)\;P(\phi-\phi_d,\psi-\psi_d)}\;.\;d\phi\, d\psi \qquad (29)$$

We then have the total power received at B

$$P_B \propto \int_{-\pi}^{\pi}\int_{-\pi}^{\pi} \sqrt{P(\phi,\psi)\; P(\phi-\phi_d,\psi-\psi_d)}\; d\phi\, d\psi \qquad (30)$$

It is convenient to normalize the power received at B so that

$$\frac{P_B}{P_A} = \frac{\int_{-\pi}^{\pi}\int_{-\pi}^{\pi} \sqrt{P(\phi,\psi)\cdot P(\phi-\phi_d,\psi-\psi_d)}\; d\phi\, d\psi}{\int_{-\pi}^{\pi}\int_{-\pi}^{\pi} P(\phi,\psi)\; d\phi\, d\psi} \qquad (31)$$

To progress further it is necessary to make a plausible assumption regarding the form of the power spectrum. We will assume that the spectrum of echoes received at the transmitter is gaussian, that is:

$$P(\phi,\psi) \propto e^{-\frac{1}{2}\left(\frac{\phi^2}{\sigma_1^2}+\frac{\psi^2}{\sigma_2^2}\right)} \qquad (32)$$

The total power received at B is then

$$P_B \propto \int_{-\pi}^{\pi}\int_{-\pi}^{\pi} e^{-\frac{1}{4}\left(\frac{\phi^2}{\sigma_1^2}+\frac{\psi^2}{\sigma_2^2}-\left(\frac{\phi-\phi_d}{\sigma_1}\right)^2-\left(\frac{\psi-\psi_d}{\sigma_2}\right)^2\right)} d\phi\, d\psi \qquad (33)$$

For receiving points in the magnetic meridian of the transmitter we have $\psi_d = 0$, and integrating with respect to ψ we have

$$\frac{P_B}{P_A} = e^{-\frac{\phi_d^2}{8\sigma_1^2}} \qquad (34)$$

A gaussian power spectrum will therefore result in a gaussian variation of Z echo power with distance from the transmitter along the magnetic meridian. By measuring the ratio $\frac{P_B}{P_A}$ and the true height of reflection h we can determine the standard deviation σ_1 of the assumed spectrum. Measurements at different distances from the transmitter would be expected to provide some indication of the validity of the assumed form of the power spectrum.

5.2 Measurements.

The ratio of the average Z echo power to the average ordinary echo power was observed at the transmitter and three other points whose relative positions are shown in Fig. 26. These positions were chosen as near as possible to the magnetic meridian through the transmitter to allow the results to be compared with the N-S D.F. measurements. For the same reason the operating frequency was 4.65 Mc/s.. E-W measurements of Z power were not practicable at Hobart because of geographical limitations.

The technique used, which is discussed in detail in Section 7.3, was to record photographically the amplitude of all weak echoes nine times per minute simultaneously at all stations. Recordings were made on an automatic basis for two hours every afternoon. On occasions when Z echoes were observed at the transmitting station the transmitter power was subsequently reduced to allow ordinary echo amplitudes to be recorded at all stations for comparison. This was done to calibrate the receivers, the assumption being that the average power of ordinary echoes was either the same at all stations or that any diversity effects affected the similarly polarised O and Z echoes to the same extent.

The detailed results of all measurements are given in Table 3.

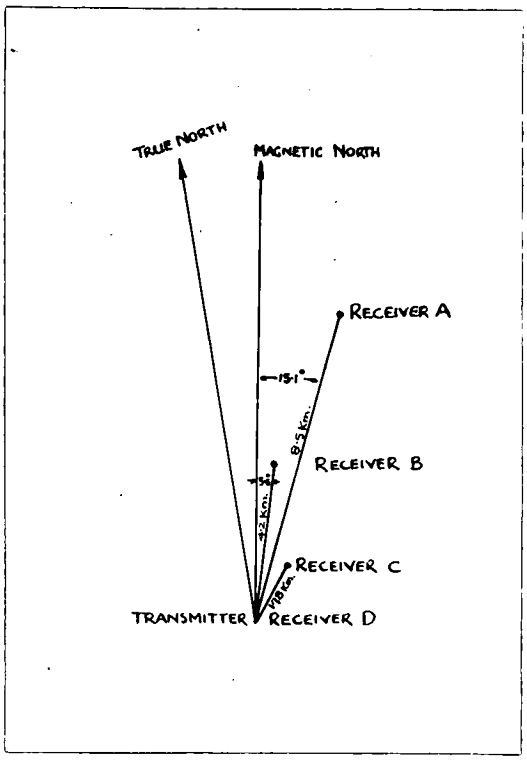

FIG. 26.

Positions of Receiving Stations.

TABLE 3.

Time	Date	No. of Observations	Normalised Value of $\frac{(X\ amplitude)^2}{(O\ amplitude)^2}$			True Height
			Receiver A	Receiver B	Receiver C	
						Km.
1800	30/3/54	54	.084	.30	.77	210
1710	2/4/54	38	.09	.23	.80	210
1735	3/4/54	61	.135	.40	.85	214
1715	4/4/54	52	.12	.28	.9	220
1800	6/4/54	98	.17	.48	.81	220
1701	22/4/54	65	.15	.42	.60	213
1710	25/4/54	30	.035	.37	-	210
1703	6/5/54	48	.07	.55	.66	205
1700	9/5/54	110	.055	.39	.68	205
1650	27/5/54	76	.14	-	.73	210
1500	5/3/54	31	-	.45	.84	202
1530	6/8/54	62	-	.31	.97	200
		Average	.084	.38	.75	210
		Standard Deviation	.046	.037	.11	

Since from equations 28 and 34, a higher level of reflection would be expected to produce an increase in the X echo power at each receiving site, it was necessary to calculate the true height of reflection for each series of observations. This was done from simultaneous h'f records by finding the true height at the frequency for which reflection of the O wave occurred at the same electron density level as the X wave at the operating frequency. It was necessary to use the ordinary wave, as only a small part of the X trace near the critical frequency was normally visible. To obtain the appropriate O wave frequency we make use of the fact that the refractive index polar diagrams near the X reflection level are nearly circular. (see Fig.16) As a result we may write

$$\int z_{oblique} = \int z_{vertical} \sec \phi_c \qquad (35)$$

That is

$$f_{o\,vertical} = \sqrt{f_{zv}^2 \cos^2\phi_c + f_{zv}\cos\phi_c} \qquad (36)$$

The actual method of calculating the true height from the P'f curve was that developed by Kelso (25) which allows for the effect of the geomagnetic field.

It can be seen from Table 3 that the true height of reflection did not vary much throughout the observations and, because of the much greater variation in the relative Z echo powers observed, it was considered that no serious error would be caused by referring all measurements to the mean height of 210 Km. The mean variation of Z echo power with radial distance from the transmitter is shown in Fig. 27.

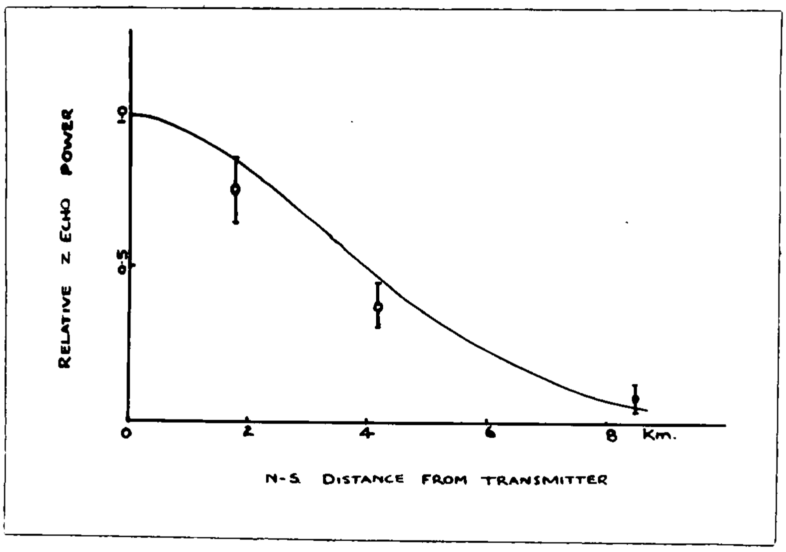

FIG. 27

Variation of Z Echo Power with Horizontal Distance from the Transmitter.

It is clear that Z echoes do return to the ground in a narrow beam as predicted by the theory. The decrease in power with distance is approximately gaussian and is therefore in reasonable agreement with the assumed gaussian form of the angular power spectrum. A gaussian curve fitted to the experimental points has a standard deviation of 3.3 Km. which, with the nominal reflection height of 210 Km., gives us 0.9° for the N-S standard deviation of the angular power spectrum.

Although a better fit to the observed points may be obtained by considering other angular power functions, it is considered that the number of points and the accuracy of the observations is not sufficient to justify detailed deductions. A gaussian spectrum may be regarded as a good first approximation.

5.3 Phase Analysis.

In analysing the distribution of the directions of arrival of Z echoes it is necessary to assume that the random fluctuations in direction are caused by multiple random scattering from irregularities within the illuminated area of the Z reflection level. This assumption has a certain amount of justification if we use the estimate by Briggs and Phillips (26) that the average size of lower F region irregularities is about two hundred metres. Since the illuminated area will be several kilometres in extent a considerable number of scattering centres would be included within it.

Consider two aerials E and F spread a distance d apart under the influence of a system of co-planar rays of the same frequency $f = \frac{p}{2\pi}$ the plane of the rays is assumed to contain the line EF. Then the voltages produced in the aerials may be written

$$V_1 = A_1 \cos(pt + \beta_1)$$
$$V_2 = A_2 \cos(pt + \beta_2) \qquad (3○)$$

The amplitude A and the phase angles β will in general be different for the two aerials. It is assumed that the phases of the component waves vary at random and independently of each other, and also that the frequency of variation is small compared with the radio frequency. The quantity observed with the direction finder is the phase difference between the voltages produced in the aerials, that is $\beta_1 - \beta_2$. We wish to examine the statistical variation of this quantity for a spread in the direction of arrival of the waves.

This problem has been investigated by Bramley (24) who showed that the relation between the phase difference probability distribution and the angular power spectrum of the waves is given by:

$$G(\alpha)\,d\alpha = \frac{1-R^2}{2\pi}\left[\frac{1}{1-R^2\cos^2\alpha} + \frac{R\cos\alpha}{(1-R^2\cos^2\alpha)^{3/2}}\left(\frac{\pi}{2}+\arcsin(R\cos\alpha)\right)\right] \qquad (38)$$

where $\alpha = \beta_1 - \beta_2 - \overline{\beta_1 - \beta_2}$

$$R = \frac{\int_{-\infty}^{\infty} P(\phi)\cos(2\pi\xi\phi)\,d\phi}{\int_{-\infty}^{\infty} P(\phi)\,d\phi}$$

$G(\alpha)$ = phase difference spectrum

$P(\phi)$ = angular power spectrum

ξ = separation of aerials in wavelengths normal to mean direction of arrival

ϕ = angle measured from mean direction

Integration of equation (38) gives the simple result

$$\overline{|\alpha|} = \frac{2\int_0^{\pi} \alpha\, G(\alpha)\,d\alpha}{\int_{-\pi}^{\pi} G(\alpha)\,d\alpha} = \arccos R \qquad (39)$$

Since R will be very nearly one we have

$$\overline{|\alpha|} \sim \sqrt{2(1-R)} \qquad (40)$$

Considering again a gaussian angular power spectrum

$$P(\phi,\psi) \propto e^{-\frac{1}{2}\left(\frac{\phi^2}{\sigma_1^2}+\frac{\psi^2}{\sigma_2^2}\right)}$$

it is first necessary to obtain the equivalent two dimensional distribution by integrating with respect to ψ giving

$$P(\phi) \propto e^{-\frac{\phi^2}{2\sigma_1^2}}$$

$$\therefore \quad R = e^{-2\pi^2\xi^2\sigma_1^2}$$

$$\sim 1 - 2\pi^2\xi^2\sigma_1^2$$

$$\therefore \quad \overline{|\alpha|} \sim 2\pi\xi\sigma_1$$

$$\text{or} \quad \overline{|\phi|} \sim \sigma_1 \qquad (41)$$

An analysis of all D.F. measurements gave:

$$\sigma_1 = 0.56^\circ = \overline{|\phi_i - \Phi_i|}$$

$$\sigma_2 = 0.45^\circ = \overline{|\psi_i - \Psi_i|}\cos\phi_c$$

(see table 2)

The N-S result is in reasonable agreement with that obtained from the power measurements, particularly since in the case of angle observations we are using a quantity $\overline{|\phi|}$, the observed value of which will be increased by any random D.F. errors. These errors are discussed in section 7.2. In the case of the power observations random errors would be averaged out in the final result. It is considered, therefore, that the result obtained from the power measurements is likely to be nearer the correct value. However, the D.F. results do suggest that the spectrum is not greatly different in the N-S and E-W directions. Summing up, we may say that, with the conditions of frequency layer height and geomagnetic field in which these measurements were conducted, the angular power spectrum of Z echoes is nearly symetrical about the mean direction with a standard deviation of about 0.37°. The corresponding half power point would lie at 0.42°.

We have seen that the narrow angular power spectrum of Z echoes may be regarded as being due to a propagation hole in the O level of reflection. Using the results of the power and phase measurements and an O reflection height of 195 Km., the hole has a gaussian section with a standard deviation of 1.6 Km. The total width of the hole to half power points is then 3.7 Km.

6. SOME APPLICATIONS OF THE Z PROPAGATION HOLE.

6.1 Back Scattering.

In the past studies of the horizontal irregularities of the ionosphere by pulse techniques have been limited by the wide beam receiver aerials used. These have allowed only measurements in which the average effect of all the irregularities over a wide area could be observed. However, the Z propagation hole in effect provides the receiver with an aerial beam width of about .84° with which we can examine at oblique incidence some of the scattering properties of a small element of the reflecting layer.

It is characteristic of many P'f records of triple splitting that the Z trace appears strongest near the Z critical frequency (See for example Fig. 28). This suggests that the power scattered back from the Z level increases as the critical frequency is approached.

This question was investigated by recording Z echo amplitudes on a fixed frequency in the way described in Section 7.3, at times when the F region critical frequency was decreasing rapidly. The ratio of the operating frequency to f_zF_2 was obtained from P'f records made every two minutes. Although it is possible to study the change in Z echo amplitude with frequency by sweep frequency techniques, it was considered that to reduce possible errors due to changes in transmitter efficiency and in ionospheric absorption with frequency, it would be better to observe the amplitude on a fixed frequency. Satisfactory observations were obtained on four occasions. These all showed an increase in the echo amplitude near the critical frequency. The results are summarised in Fig.29.

The reason for this effect is not obvious, although one may suppose that at oblique incidence, when the critical frequency is approached, the wave group will travel a greater distance horizontally, encountering more irregularities than when the frequency ratio $\frac{f}{f_c}$ is much lower.

The increased back scattering would normally affect measurements using the ordinary or extraordinary waves at frequencies above their respective vertical incidence critical frequencies, for example, in investigations of spread F echoes. At these frequencies all echoes may be due to oblique back scatter and the enhancement of the echo power would modify their angular power spectrum.

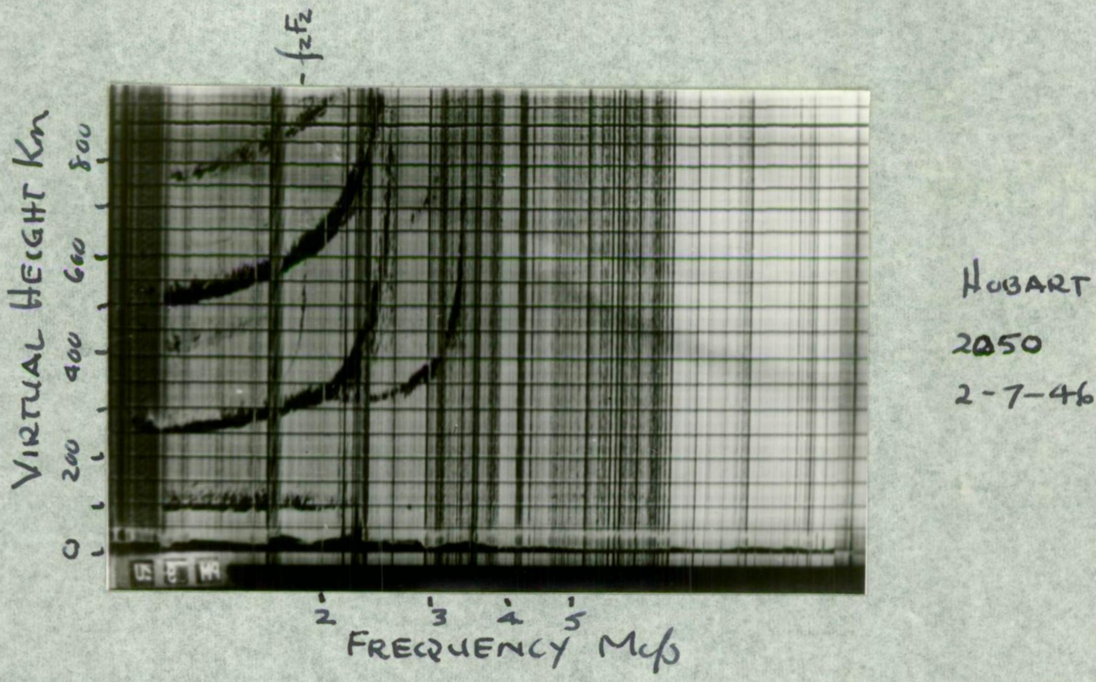

FIG. 30

P'f Record showing enhanced Z Trace near f_zF_2.

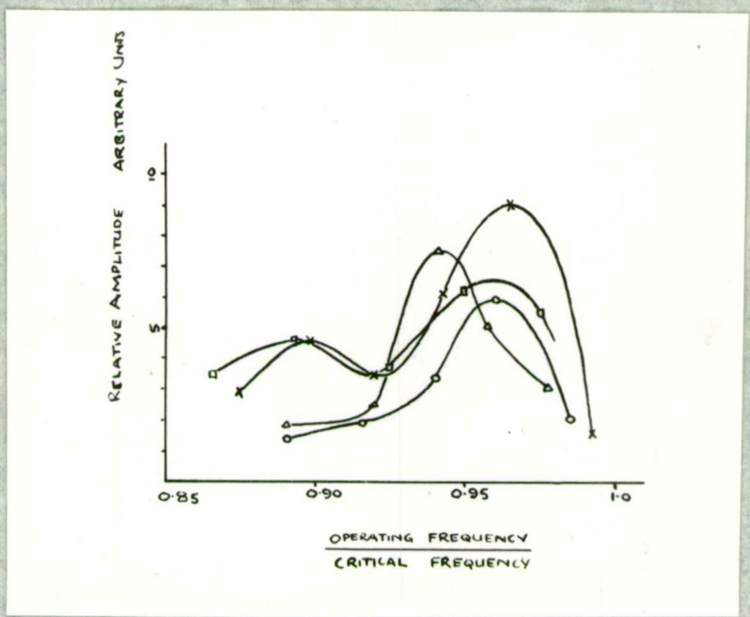

FIG. 31

Variation in Z Echo Amplitude near the Critical Frequency.

6.2 Z Critical Frequency.

An interesting property of the Z trace on P'f records is that it forms an easily measured frequency reference from which the vertical incidence ordinary wave critical frequency can be calculated when its value is doubtful because of severe critical frequency spreading. Using Equation 36 we have for the vertical incidence O-wave critical frequency

$$f_{o_{crit.}} = \sqrt{f_{z_{crit.}}^{2}\cos^{2}\phi_c + f_{z_{crit.}} f_H \cos\phi_c} \qquad (42)$$

Figs. 31, 32 and 33 show some examples of P'f records of spread F ionospheric echoes. It can be seen that the calculated value of f_oF_2 falls either near the inside edge of the O trace or at a somewhat higher frequency. These two situations are typical at Hobart, the former being most frequently observed. In this case it appears that the spreading is entirely due to oblique backscatter.

In the second situation it appears from P'f records taken at Hobart every ten minutes that the spreading below the calculated value of f_oF_2 is recorded as an additional trace which gradually spreads towards the O trace. It is possible, therefore, that it is caused by oblique backscatter from a region of less maximum electron density than occurs at vertical incidence.

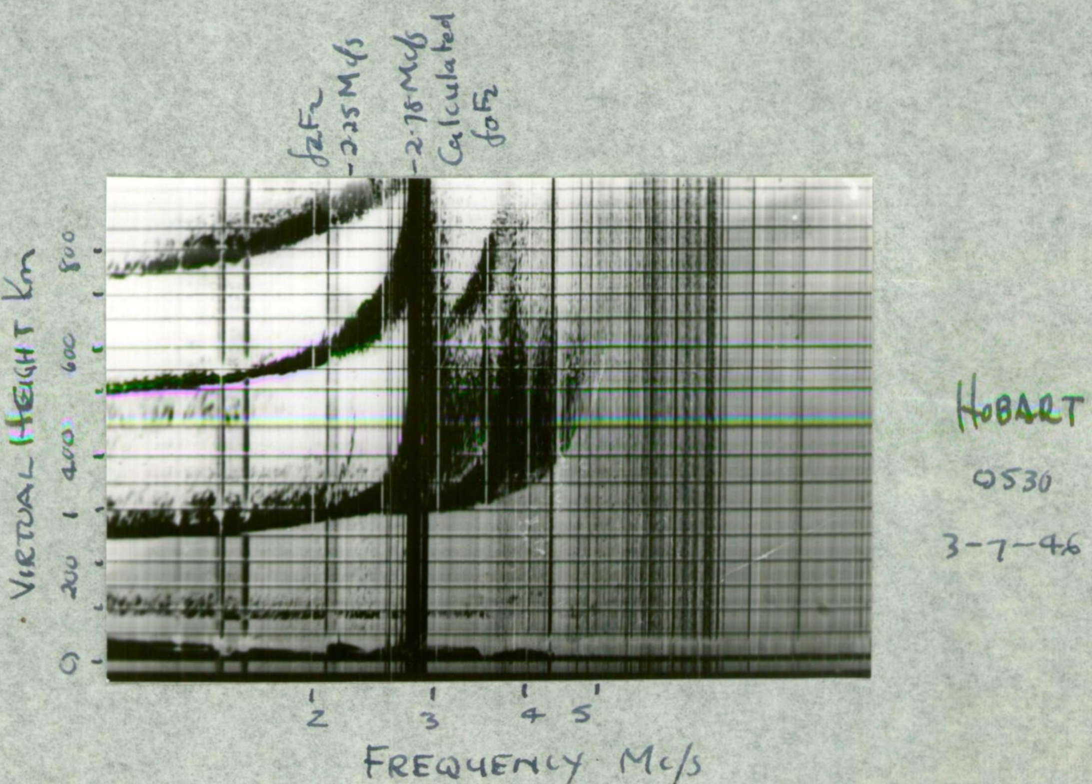

FIG. 31.

P'f Record Showing Spread F Echoes.

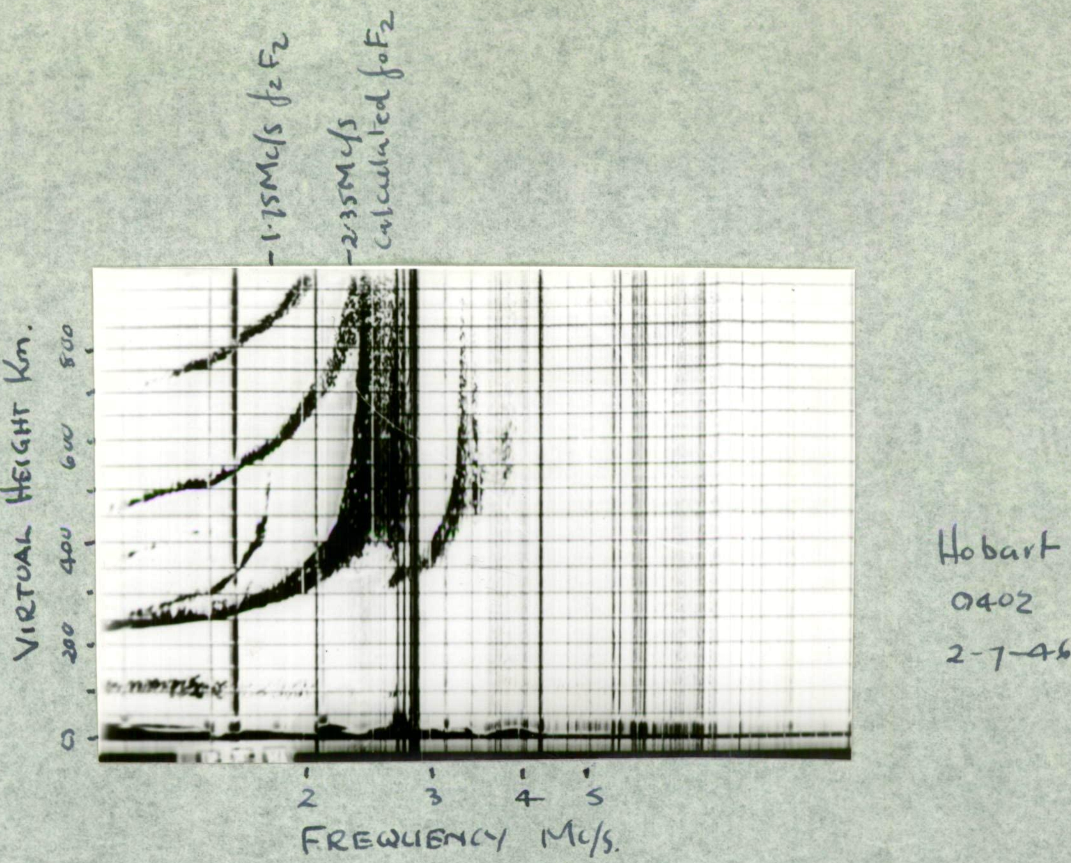

FIG. 32.

P'f Record Showing Spread F Echoes.

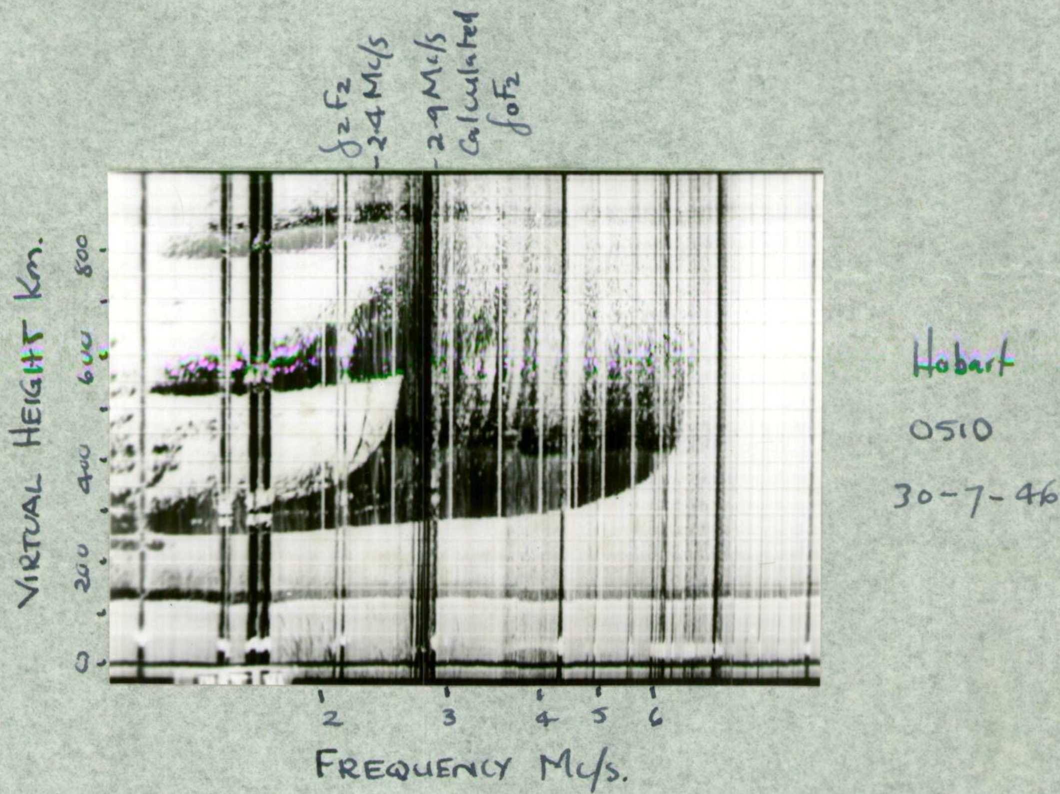

FIG. 33.

P'f Record Showing Spreading below the Calculated Value of f_oF_2.

6.3 Radio Astronomy.

An interesting possibility of using the Z propagation hole lies in the field of radio astronomy. By choosing the operating frequency above the Z critical frequency, waves which have penetrated the Z hole in the O level will not be reflected at the Z level, but will penetrate the electron maximum of the layer. Between the Z and O critical frequencies neither the X or O waves will pass through the layer which will form a reflecting screen, except in the direction of the hole. For complete penetration of the layer the up-going or down-coming O wave would have to penetrate a second Z hole at the ordinary level of reflection above the electron maximum. The approximate ray paths are shown in Fig.34. We, therefore, have the possibility of examining extra-terrestrial radio sources at frequencies of a few megacycles with an effective receiver beam width of about $.84^{\circ}$.

It is necessary first to consider whether the differences in geomagnetic field strength and magnetic dip between the upper and lower O levels is sufficient to cause misalignment of the two holes. Fortunately, this does not occur for typical F region electron distributions. The case considered in Figs. 35 and 36 gives a maximum difference in direction for the two holes of $0{\cdot}16^{\circ}$

We will illustrate the procedure of using the propagation hole by considering the case of observations from points near the Greenwich meridian of the radio sources in Cygnus (R.A. 19 hr. 58 min. Dec. $40\frac{1}{2}^{\circ}$). From the curve of the variation of the zenith angle of Cygnus with geographic latitude as it crosses the magnetic meridian we find the necessary direction of the propagation hole at each latitude. Using the appropriate values of F region magnetic dip and field strength, we then obtain the variation of operating frequency with geographic latitude from Equation 25

$$\sin\phi_c = \sqrt{\frac{Y}{1+Y}}\ \sin\Theta_c \qquad (25)$$

For example, at latitude 51.5° N. and with an operating frequency of 3.25 Mc/s the direction of the propagation hole will coincide with the direction of Cygnus when it crosses the magnetic meridian.

Because the propagation hole has an angular width of $\cdot 84^{o}$ the operating frequency can lie between 3.2 and 3.3 Mc/s without seriously affecting this result.

In Southern Englandappropriate critical frequencies will occur only during the night. This limits the months of observation to those when Cygnus crosses the magnetic meridian during the early hours of the morning, that is, during June and July. However, by varying the latitude of the place of observation, the operating frequencymay be chosen to lie near the probable F region critical frequency at any time of the day .

Cygnus has been chosen as an example, because it is a strong source in the presence of a relatively weak background, and would seem to afford the best hope of testing the technique.

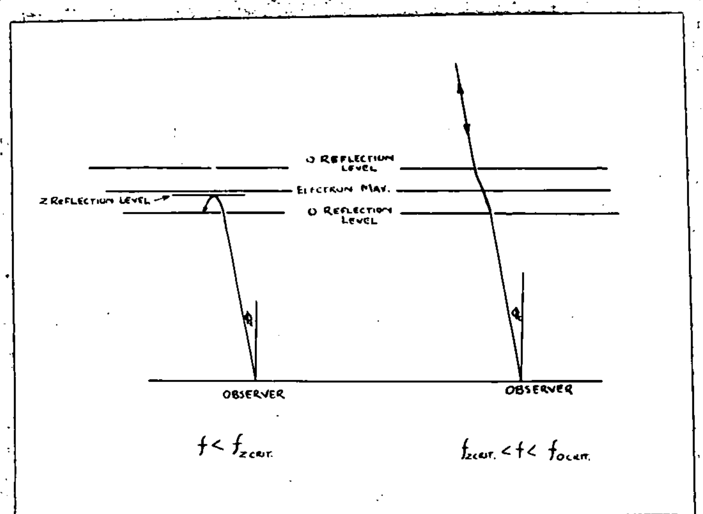

Fig. 34.

Approximate ray paths.

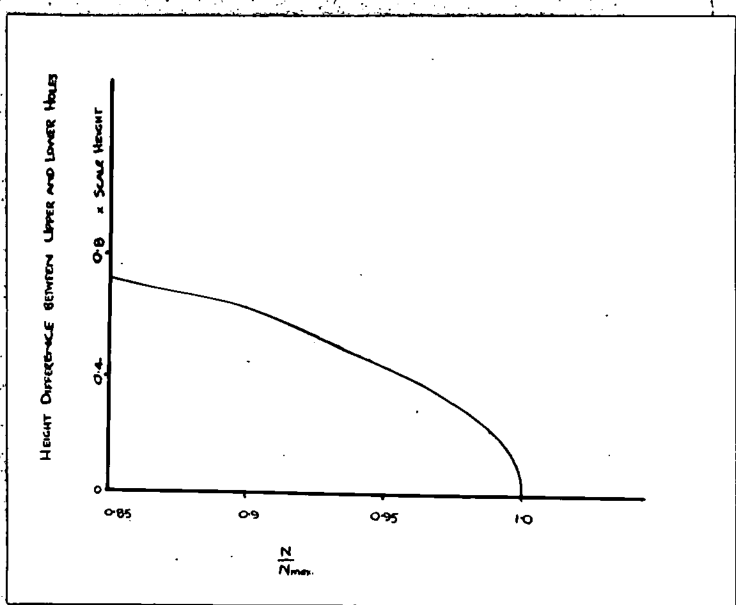

Fig. 35

Height difference between upper and lower holes.

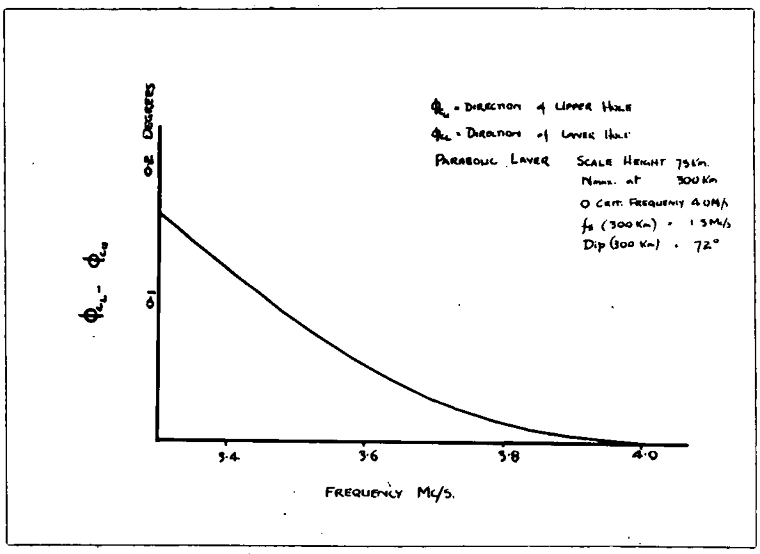

(Dipole field)

Fig. 36.

Difference in mean direction of upper and lower holes.

Some limitations to the technique may be summarised as follows:-

(a) It is not known to what extent the incoming wave would be attenuated by operating so close to the critical frequency. Measurements by Shain & Higgins (27) on 9.15 Mc/s. and 18.3 Mc/s have suggested that the increase in attenuation as the critical frequency is approached, is greater than would be expected from simple magneto-ionic theory.

(b) Although the propagation hole provides the receiver with comparatively high angular resolution, there is no increase in the signal to noise ratio such as would be obtained with a narrow beam aerial. For night measurements in the summer the effect of atmospherics would probably be the limiting factor unless a reasonably directive aerial were used.

(c) At any given latitude a strip of the sky only a few degrees wide can be scanned by the hole.

Although no strong sources have been found at a suitable declination for observation from Hobart, the galactic centre passes near the propagation hole in the early hours of the morning during months of May, June and July. At these times measurements made during 1954 at Hobart have shown that interference from atmospherics is often very small, and it is possible that there may be sufficient radiation from the galaxy for successful observations. It is also possible that there are strong sources near the galactic centre which would not have been discovered by interferometer techniques because of the strong background radiation.

These ideas will be tested by observations to be made at Hobart during the coming winter.

6.4 Ionospheric Roughness.

Since F region Z echoes are entirely due to backscattering, it is obvious that they provide evidence of irregularities in the reflecting layer. Also, since they are due to backscattering from a small element of the layer, their amplitude is a direct indication of the degree of roughness of the layer. It is interesting, therefore, to examine how the occurrence of Z echoes is related to estimates of the ionospheric roughness obtained in other ways.

A method of estimating roughness, using pulse techniques, has been developed by Briggs and Phillips (26) who showed that the angular spread of downcoming waves may be related to the difference correlation coefficient between the amplitude fading patterns at two points on the ground. They assumed that the angular power spectrum of echoes received at the transmitter from a rough ionospheric layer is approximately gaussian, that is:

$$p(\phi) \propto \cos^m \phi \qquad (43)$$

In this case the parameter m of the power spectrum may be related to the average correlation between values of the echo amplitudes $A_1 A_2$ measured at two points on the ground ξ wave lengths apart, by the expression

$$\rho_A(\xi) \propto \left[\int_{-1}^{1} (1-s^2)^{\frac{m}{2}} \cos(2\pi\xi s)\, ds \right]^2 \qquad (44)$$

where

$$\rho_A(\xi) = \frac{\overline{A_1 A_2} - (\bar{A_1})^2}{\overline{(A_1)^2} - (\bar{A_1})^2} \qquad (45)$$

In practice, instead of $\rho_A(\xi)$ it is more convenient to measure the difference correlation $\Delta(\xi)$ where $\Delta(\xi)$ is given by

$$\Delta(\xi) = \overline{|A_1 - A_2|} \qquad (46)$$

and

$$\frac{\Delta(\xi)}{\bar{A}} = 0.59\left(1 - \rho_A(\xi)\right)^{\frac{1}{2}} \qquad (47)$$

(see McNicol (32))

Also, instead of using parameter m we may define a parameter ϕ_0, the quarter power angle in the received spectrum, that is

$$\cos^m \phi_0 = \frac{1}{4} \qquad (48)$$

Briggs and Phillips showed from Equations 44, 47 and 48 that $\frac{\Delta(\xi)}{\bar{A}}$ is approximately proportional to ϕ_0 providing ϕ_0 is less than about 10° and ξ is less than one wavelength. In the case of $\xi = \frac{2\lambda}{3}$ for example, where ϕ_0 is measured in degrees, we have

$$\phi_0 = 40\frac{\Delta(\xi)}{\bar{A}} \qquad (49)$$

Measurements of $\frac{\Delta(\xi)}{\bar{A}}$ were made at Hobart during July and August, 1953, using the twin channel amplitude recorder attached to the direction finder (See Section 7.2.3). The amplitudes recorded were of ordinary echoes received in the North and South loops respectively. The wave frequency was 5.8 Mc/s and the spacing ξ between the loops was $\frac{2}{3}$ wave lengths. All measurements were made between 1300 and 1800 hours. The results are summarised in Table 4. Occasions when triple splitting was recorded by the P'f recorder are also shown.

TABLE 4.

	ϕ_0 Degrees								
	0 - 1	1 - 2	2 - 3	3 - 4	4 - 5	5 - 6	6 - 7	7 - 8	8 - 9
Number of Observations	5	9	13	11	11	5	3	4	1
Number of Times Triple Splitting Recorded Simultaneously	0	0	0	0	5	4	1	3	1

It can be seen that there is a good qualitative agreement between the occurrence of triple splitting and increased ionospheric roughness as indicated by observations of Φ_o , particularly since the technique of measuring roughness is very approximate. The assumed form of the power spectrum does not take account of the axial asymmetry about the vertical of oblique reflection, which is due to the presence of the geomagnetic field. Also, the enhancement of Z echoes near the critical frequency, reported in Section 6.1, would produce observable triple splitting at smaller values of Φ_o than otherwise would be expected. Because of these factors it was not considered useful to attempt a more detailed correlation between the occurrence of Z echoes and ionospheric roughness.

7. EXPERIMENTAL TECHNIQUES.

7.1 Polarisation Measurements.

In the investigation of the polarisation of Z echoes it was necessary only to determine the sense of polarisation. Detailed knowledge of the elliptical polarisation of the echoes was not of great interest. Also, because of the circumstances at the time, it was desirable to use a system of measurement which could be made automatic. These conditions were met by using a circular polarisation receiver of a type due to Pulley(28).

7.1.2. Principle of measurement.

Pulley's system essentially is equivalent to electrically rotating a loop aerial about a vertical axis at a high audio frequency. A circularly polarised down-coming wave will then produce in the aerial a current of frequency less than or greater than that of the wave frequency, depending on whether the rotation of the wave field vector is in the same or in opposite sense to the rotation of the loop. By connecting the aerial to a receiver tuned either above or below the wave frequency, signals due to waves of opposite polarisations can be separated.

The actual method of effectively rotating the aerial is to use two loops mounted vertically at right angles to each other. They are connected to the grids of four valves which are modulated in phase quadrature at about 30 Kc/s. The outputs of the four valves are connected in parallel to a pulse receiver. The method of modulation causes each of the modulating valves to conduct successively in a cyclic manner. The effect is equivalent to rotating a single loop aerial at the modulation frequency.

7.1.3. Theory of Operation.

With a pair of typical sharp cut-off valves, such as the 6SK7, connected with the grids in push-pull and the plates in parallel, the resultant mutual conductance will be linear providing that the steady bias is suitably chosen. With a small value of load impedence compared with the valve impedence, the mutual conductance is a measure of the amplification factor of the stage, that is, we can write

$$\mu = KE_g$$

μ = amplification factor
E_g = voltage on grid
K = constant

A small voltage E_1 in addition to the steady bias and a modulating bias E_g will produce $E_1 kE_g$ across the anode circuit. If E_g is of the form $V\cos\omega t$ then the resultant voltage across the anode circuit will be $E_1 V\cos\omega t$ for one pair of valves and $E_2 V\cos\omega t$ for the other pair, since the modulating voltage is 90° out of phase in this case.

Suppose that a circularly polarised wave is incident on the loops in a vertical direction, so that

$$E_1 = A\cos pt \quad , \quad E_2 = A\sin pt$$

The resultant voltage in the anode circuit will be

$$KVA(\cos pt\cos\omega t + \sin pt\sin\omega t)$$

$$= KVA\cos(p-\omega)t \qquad (50)$$

We see that the frequency of the signal has been reduced by an amount equal to the modulating frequency. If the incident wave had been circularly polarised in the opposite direction then

$$E_2 = -A\sin pt$$

and the output becomes

$$KVA(\cos pt\cos\omega t - \sin pt\sin\omega t)$$

$$= KVA\cos(p+\omega)t \qquad (51)$$

In general, whatever the state of polarisation of the wave or its angle of incidence, the projection of the magnetic vector on the horizontal plane will be the only component which will affect the loops, and this projected vector can in turn be resolved into two rotating vectors with opposite senses of rotation. One of these vectors will produce currents in the anode circuit equal to the difference and the other equal to the sum of the signal and modulation frequencies. No current of the original signal frequency appears in the anode circuit and, since the receiver is tuned to the heterodyne frequency, no error will be caused by signal frequency pick-up in the leads or receiver.

7.1.4. Details of Apparatus.

Figs. 37 to 41 show the block diagrams and circuits of the various pieces of equipment. To avoid retuning the receiver to the upper and lower heterodyne frequencies the sense of modulation was reversed by means of a switch. A synchronously operated switch in the output of the receiver allowed echoes of opposite polarisation to be displayed on the two beams of a double beam oscilloscope. The receiver was a communications receiver with its band width increased to 25Kc/s with resistors across the IF circuit. The receiver aerials were single turn shielded loops 2'6" in diameter with a tuning range of 2.2 to 4 Mc/s. The pulse transmitter was of conventional type with a peak power of 4 Kw., a pulse length of 100 μ.sec. and a pulse repetition frequency of 50 per second.

The display oscilloscope was photographed with an intermittently operated camera, using 35 mm. film.

Observations were made automatically once hourly on a frequency of 2.3 Mc/s. The normal sequence of operations was as follows:

1. Pulse transmitter on.
2. Cathode ray oscilloscope on.
3. P'f recorder on.
4. Camera shutter opened for [illegible] second.
5. Polarisation switch reversed.
6. Camera shutter opened for [illegible] second.
7. Polarisation switch to normal.
8. P'f recorder off.
9. Film wound on.
10. C.R.O. and transmitter off.

The whole sequence took approximately eight minutes. All switching was carried out by cams and spring sets for low current circuits and cams and mercury switches for high current circuits. Automatic recording was necessary during these observations because P'f records necessary for identification of echoes were available at the time only once hourly. Typical photographs produced by the apparatus show clearly the sense of polarisation of ordinary and extraordinary echoes.

7.1.5. Consideration of Errors.

The main errors in equipment of this type are due to improperly tuned loops or to incorrect adjustment of the modulating circuit. Pulley has shown that such errors in adjustment will reduce the discrimination of the receiver against the unwanted polarisation. He gives an elaborate procedure for arriving at the correct adjustment. However, since in this investigation only the sense of polarisation of Z echoes was required, the receiver was simply adjusted to give maximum discrimination against ordinary and extraordinary echoes, depending on the position of the polarisation switch. As we have seen in Section 2, observations with the equipment showed that Z echoes are polarised in the same sense as ordinary echoes.

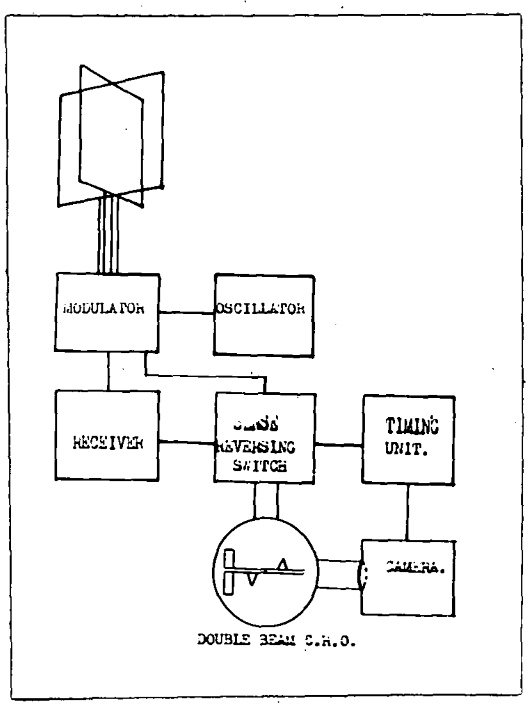

FIG. 37.

Schematic Diagram of Polarisation Receiver.

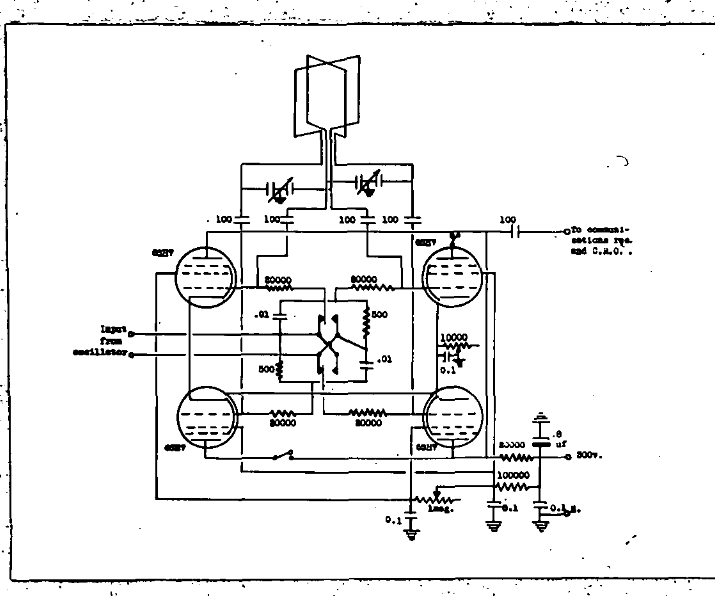

FIG. 38. Circuit Diagram of Polarisation Discriminator.

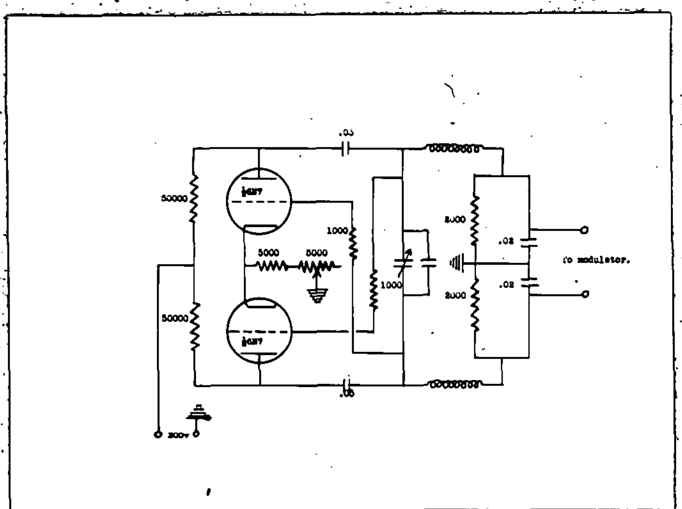

FIG. 39. Circuit Diagram of Modulating Oscillator.

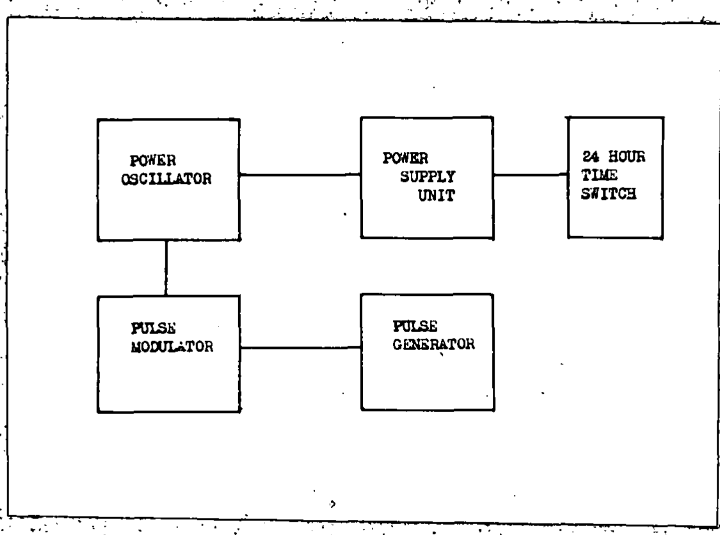

FIG. 40. Block Diagram of Transmitter.

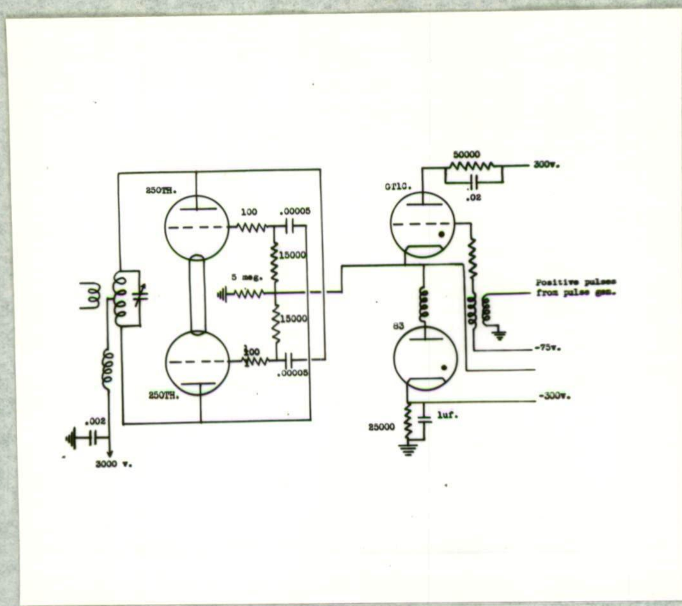

FIG. 41. Circuit of Transmitter Power Oscillator

3.3 Mc/s

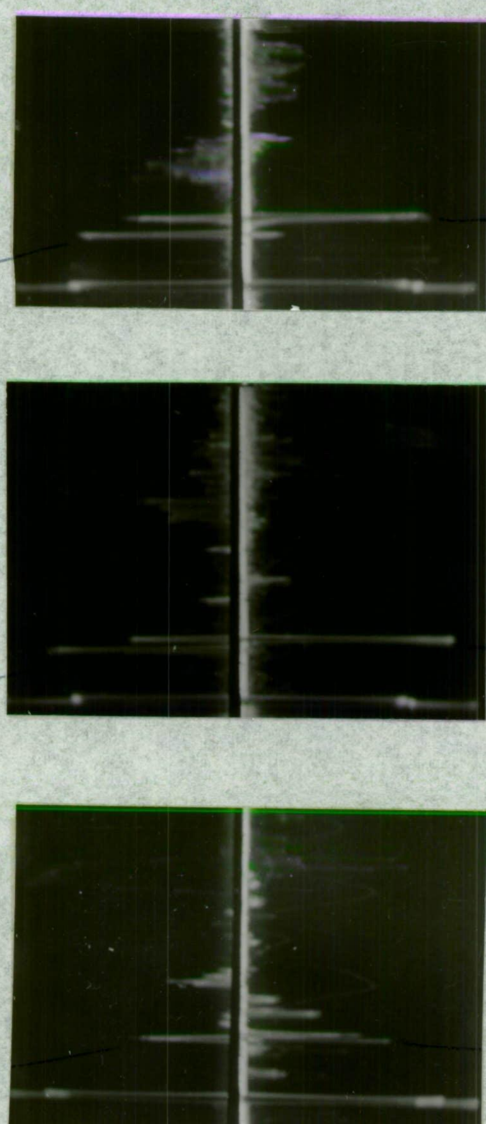

FIG. 42. Typical Polarisation Records.

Left Handed Polarisation　　　　Right Handed Polarisation.

7.2 D. F. Measurements.

To measure completely the direction of arrival of radio waves reflected in the ionosphere it is necessary to measure at least two independent parameters from which the direction in space may be derived. One of the most accurate methods available is to measure the phase differences between the signals induced by the down-coming waves in at least three spaced aerials. In practice it is most convenient to use four aerials arranged at the corners of a square as in Fig.43. The phase differences between diagonally opposed pairs of aerials are measured. This method has been used in the past by Eckersley (29) and Ross et al (19).

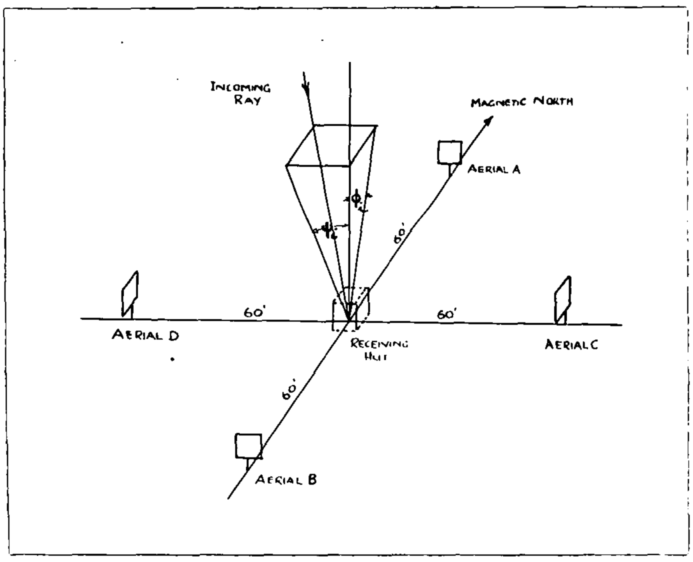

FIG. 43.

Co-ordinate System for D.F. Measurements.

7.2.1 Principles of Measurement.

Consider four aerials A.B.C.D. We choose an angular co-ordinate system based on the vertical planes through A.B. and C.D. Let ϕ_i be the projected vertical angle of arrival on plane A.B. and ψ_i the corresponding quantity on C.D. Then if α_1 is the phase difference between any chosen component of the field of a plane wave at aerials A and B and α_2 is the phase difference between C and D, we have

$$\alpha_1 = \frac{2\pi g}{\lambda} \sin\phi_i$$

$$\alpha_2 = \frac{2\pi g}{\lambda} \sin\psi_i \qquad (52)$$

g = distance between pair of aerials
λ = wavelength.

If the aerials have no mutual reactions on each other then the phase differences between the signals in aerials A and B and in C and D will also be $\alpha_1 + \alpha_2$. ϕ_i & ψ_i may then be deduced from the measured values of $\alpha_1 + \alpha_2$

It may be noted that the resolving power of the aerials defined as the rate of change of phase difference with respect to direction of arrival will be a maximum at vertical incidence, that is

$$\frac{\partial \alpha_1}{\partial \phi_i} = \frac{2\pi g}{\lambda}\cos\phi_i \qquad \frac{\partial \alpha_2}{\partial \psi_i} = \frac{2\pi g}{\lambda}\cos\psi_i \qquad (53)$$

It will be zero for each pair when the waves arrive in the direction of the line joining the pair.

7.2.2. Phase Measurements.

The phase measuring equipment is required to indicate in a manner suitable for recording, the phase difference between RF signals of nearly equal amplitude. Although methods (see for example (19)) have been developed for displaying the phase difference directly on a CR tube, it was decided in the interests of simplicity to use the well known technique of applying the amplified signals directly to opposite pairs of plates of the tube.

Suppose that two sine wave voltages $V_1 = A_1\cos(pt+\beta_1)$, $V_2 = A_2\cos(pt+\beta_2)$ proportional to the incoming wave electric vector amplitudes are applied to the vertical and horizontal deflection plates respectively. The deflection of the spot will be given by

$$x = K_1 V_1 \qquad y = K_2 V_2 \qquad K_1, K_2 \text{ constants}$$

If the phase difference between V_1 and V_2 is α an ellipse will be produced which is bounded by a rectangle with sides

$$X_1 = 2K_1A_1 \qquad Y_2 = 2K_2A_2$$

Since the ellipse cuts the horizontal axis at distance $\frac{X_1}{2}\sin\alpha$ from the origin we have

$$\sin\alpha = \frac{a}{K_1A_1} \qquad a = x \text{ intercept of ellipse} \qquad (54)$$

In practice it is more convenient to measure $\frac{2a}{X_1}$ since this does not involve finding the centre of the ellipse. An alternative method is expressed by

$$\sin\alpha = \frac{e \cdot f}{X_1 Y_2} \qquad \text{where } e, f \text{ are the major \& minor axes of the ellipse}$$

However, it has been shown (Benson and Carter (30) that for a given size spot and ellipse the maximum errors of the second method will be nearly twice those of the first.

7.2.3. Details of Apparatus.

(i) Aerial System.

The aerials used were single turn screened loops four feet square. They were mounted on concrete foundations with their lower limbs about three feet above the ground. They were connected via cathode followers and twin shielded cable to the receiving hut. Balanced tuning condensers across the loops gave a tuning range of 3.5 to 7.5 Mc/s. The feeder cables were buried one foot in the ground and the cathode followers were fed with power by buried wires alongside the RF cables. A coupling unit between the feeders and the receiver allowed any two loops to be connected to the receiver at one time. The mains cable was fed to the receiving hut in a trench 1'6" deep running along the line of one aerial pair. The whole system was situated approximately 1,000' from the pulse transmitter which has already been described in Section 7.1.4.

(ii) Receiver.

A modified Admiralty type FHB twin channel cathode ray DF receiver was used. This receiver was capable of independently amplifying and converting to IF frequency, two RF signals without appreciably altering their relative amplitudes and their phase difference. Two similar superheterodyne amplifiers were used with a common frequency changing oscillator. The IF outputs were connected to the CR tube plates. The receiver included a test oscillator for lining up all stages. The general functional lay-out of the installation is shown in Fig.44 and the basic circuits in Figs. 45, 46 and 47. The IF band width was increased to 20 Kc/s with damping resistors.

(iii) Cathode Ray Tube.

The cathode ray tube was a 7" diameter electrostatic tube with green flourescent screen of medium persistence. The geometrical accuracy of the tube was such that the angular error of position of the spot did not exceed $\frac{1}{4}^{\circ}$. The diameter of the spot did not exceed 1 mm. with moderate brilliance. Distortion of the ellipse due to inaccurately aligned electrodes was therefore less than one quarter line width for ellipses of 6 cm. major axis or less. A Cossor oscillograph camera, using 35 mm. film, was used to photograph the screen.

Since 100 usec. pulse transmissions were used it was necessary to eliminate all echoes except the wanted ones from the CR tube. This was done by gating the tube with pulses of adjustable width and delay from a pulse generator triggered by the ground wave of the transmitter.

Also, it was necessary to know the sense in which the ellipse was traced on the screen to determine the sign of the phase difference. To resolve this ambiguity part of the IF signal was fed into a separate IF amplifier and then applied to the CRT grid. By tuning the external IF amplifier to produce a 45° phase change in this signal a dark spot could be produced on one side or other of the ellipse, depending on the sense of rotation

(iv) Gating Pulse Generator.

The pulse generator was of conventional type, using monostable multi-vibrators to produce both the time delay and the variable width of the gating pulse. The delay time, after triggering by the transmitter ground wave, could be varied from one millisecond to five milliseconds. This range covered all F region echoes. The gating pulse could be varied in width from 20 to 200 microseconds. Generally, a hundred microsecond pulse was used. The audio output of the receiver was fed to a separate CRO to give a type A display which showed the position in time of all echoes, together with the position of the gating pulse.

(v) Amplitude Recorder.

Part of the signal in each IF channel of the receiver was amplified externally, detected and fed into a double beam CRO. The cathode ray tube of this oscillograph was also gated to display on the screen the selected echo amplitude in each channel. The screen was photographed, using continuously moving 35 mm. film.

7.2.4. Operation of the Receiver.

The accuracy of the phase difference measurements with a receiver of this type is limited by the accuracy with which the gain and phase shift of the two channels can be established and maintained. There were incorporated in the receiver a system of switches and variable capacitors for this purpose.

The preliminary adjustment was carried out stage by stage commencing at the output. The signal grids of the output valve were connected together and a test signal injected into the RF stages. The output IF transformers were adjusted to resonance, that is, maximum voltage gain. Since the rate of change of amplitude is zero at resonance, while the rate of change of phase is a maximum, this method also provided a means of compensating for the small phase inequalities in the non-tunable parts of the circuit without appreciably altering the amplitude balance. All preceding stages, except the input, were adjusted successively in the same way. To balance the input stages a battery test oscillator was used to radiate a calibrating signal into the loop aerials from a point equi-distant from a given pair of aerials.

7.2.5. Stability of the Balance Adjustment.

The receiver was not temperature compensated and consequently an initial drift of the frequency of the mixer oscillator and of the resonant frequencies of the other tuned circuits occurred during the first few hours after switching on. However, this drift affected both channels simultaneously and balance errors were, therefore, of the second order. During a series of observations the overall balance was checked with the battery oscillator every fifteen minutes. Changes in the balance were sometimes found amounting to a phase error of up to 2°. On these occasions it was assumed when scaling the film that the drift had taken place linearly between successive checks.

7.2.6 Errors.

(i) Systematic Errors.

Any inaccuracy in lining up the system would produce a systematic error in the observed direction of arrival. It was found that the test oscillator placed at different positions along the right bisector of the line joining either pair of loops did not give identical line-up results at all points. There was, therefore, a residual lining-up error which was constant at any particular frequency. On the N-S pair of aerials the difference corresponded to 1.3° in direction between points 100' East and 100' West of the receiver hut. A systematic error could also be caused by slope of the site which in this case was 0° E-W and $1\frac{1}{2}$° from South to North downwards.

The total site and lining-up errors for the actual position of the test oscillator were estimated by making a series of observations of the direction of arrival of F region ordinary echoes. The results obtained were

No. of Observations	Mean direction
72	0.45° N.
65	0.62° E.

It was assumed that the mean direction of arrival of these echoes was vertical.

(ii) Random Errors.

(a) Phase Measurements.

The accuracy of measuring phase difference by the ellipse method assuming pure sine waves is limited by the finite width of the ellipse line. In the present case the ellipse was photographed and the film projected in a film reader. The thickness of the line was generally about $\frac{1}{25}$ of the major axis of the ellipse. The dimensions were measured to the centre of the line. The errors involved in measuring the ellipse were estimated by projecting it and marking the appropriate dimensions on blank paper. These were measured with dividers and rule. On a typical ellipse the RMS error over forty such measurements corresponded to 0.14° in direction. Another determination on a larger ellipse gave 0.125°. The corresponding phase difference errors were 0.51° and 0.45° respectively.

(b) Site Errors.

At oblique incidence a major contribution to random phase errors is caused by re-radiation from a large number of obstacles scattered over an area within several kilometres of the receiver. However, with angles of arrival near vertical incidence, such errors will be very small and negligible in comparison with errors in phase measurement.

(c) Aerial Coupling Errors.

It is only when the aerials have no mutual impedence that the phase difference between the currents in opposite aerials is equal to that between the wave field at the same points. In practice coupling between the aerials may be reduced to a negligible amount by using screened loop aerials placed broadside on and separated by at least half a wave length. This was done in the installation described here by establishing the base line and the direction of one loop with a theodolite and then orientating the second loop parallel to the first by sighting on distant objects.

7.2.7. Method of Observation.

When measuring the complete direction of arrival it was necessary to observe directions in the N-S vertical plane and in the E-W plane successively, by switching the loops. As a result a complete observation took about 25 seconds. The camera was operated manually. When measurements of only the N-S or the E-W component of direction were made one photograph was taken every 15 seconds. Figs. 48 and 49 show typical examples of Z echo ellipses.

Observations were made manually and, since it was necessary to isolate the Z echo from the O and X echoes, only a short time was available for observations on each occasion. At Hobart, F region Z echoes can normally be resolved over a frequency range of only a few hundred kilocycles below the Z critical frequency and, as a result, the measurement time was limited to that taken by the F region critical frequency to change through this range. D.F. measurements were generally possible only for about ten minutes, although on a few occasions the Z echo could be followed for about half an hour. The usual method of observation was to have the direction finder ready to operate during each afternoon on a frequency below the average maximum day time critical frequency. The slow decrease in critical frequency during the afternoon would then bring any resolvable Z echoes into the direction finder operating frequency.

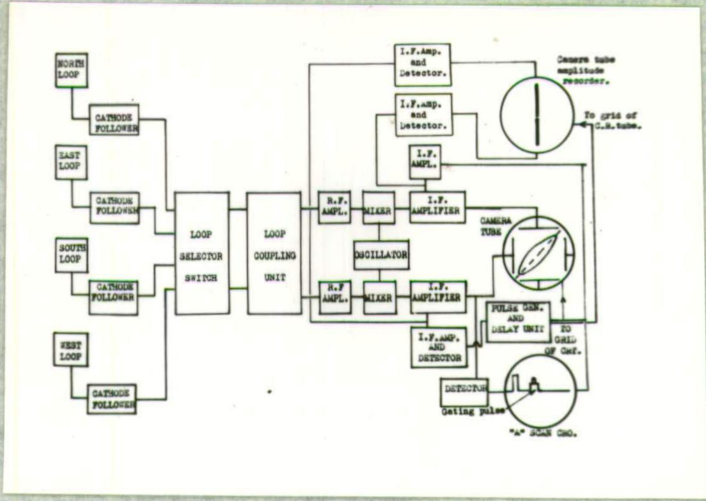

FIG. 44.

Block Diagram of Direction Finder.

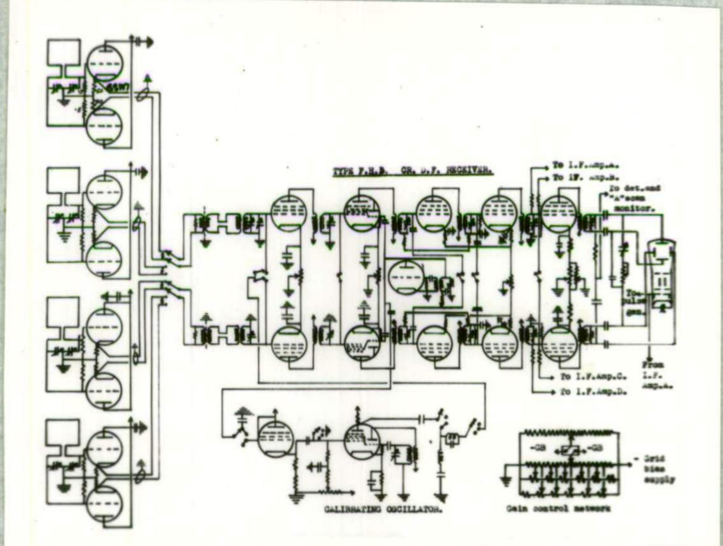

FIG. 45.

Circuit of D.F. Receiver.

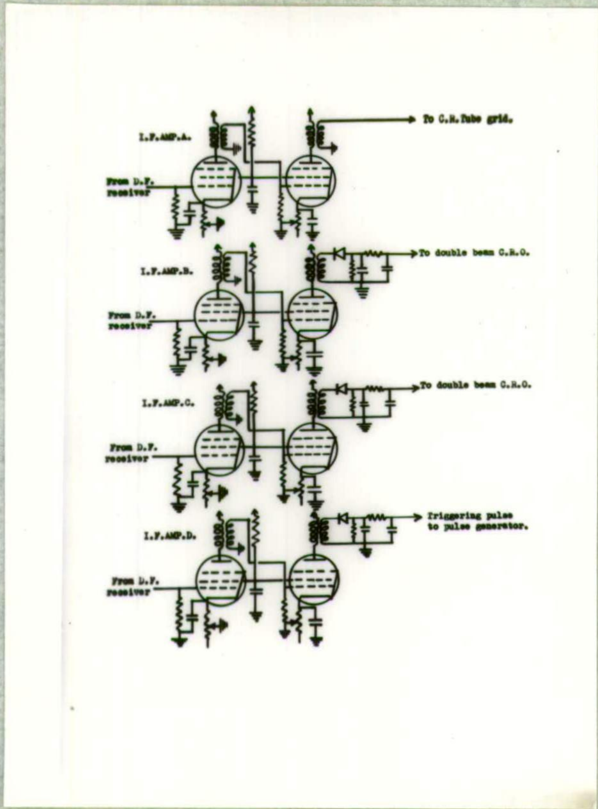

FIG. 46.

Circuit of Outboard I.F. Amplifiers.

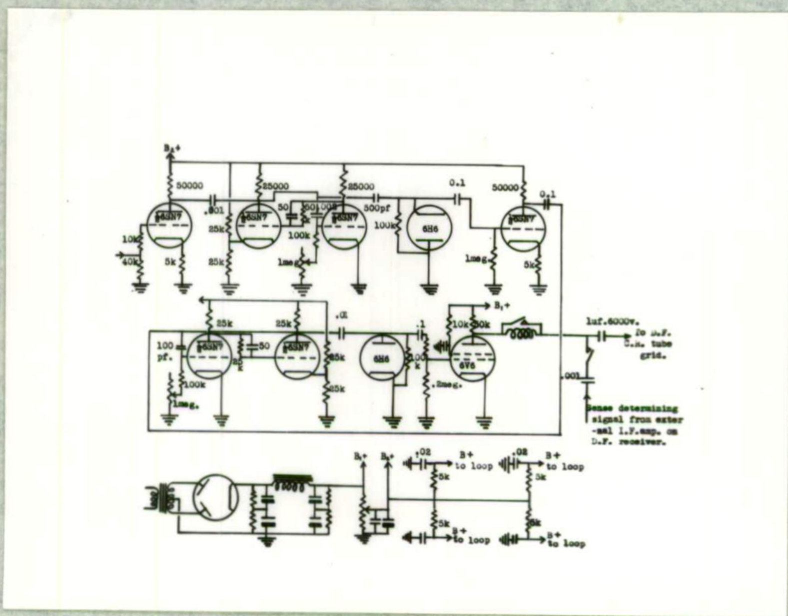

FIG. 47.

Circuit of Gating Pulse Generator.

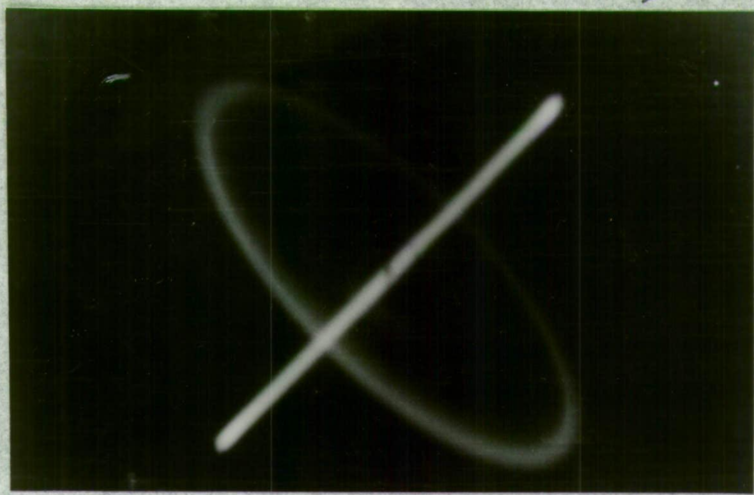

FIG. 48.

Z Echo N.S. and E.W. Ellipses.

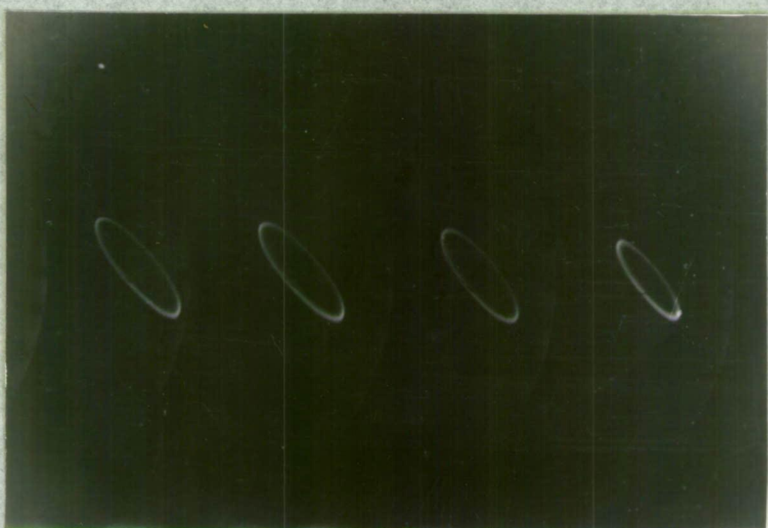

FIG. 49.

Series of Z Echo N.S. Ellipses.

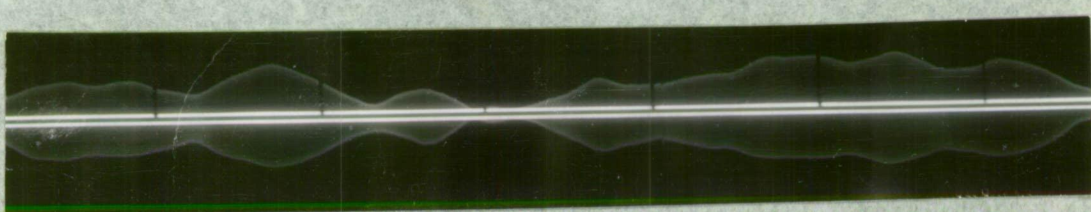

FIG. 49 a.

Twin Channel Amplitude Fading
Pattern of Ordinary Echoes.
(Time marks 10 seconds apart).

7.3 Amplitude Measurements.

In measuring the amplitude of echoes simultaneously at four places the manual system of continuously recording the amplitude of a selected echo is not suitable. Instead, it is necessary to use an automatic method, the simplest being that of recording the amplitudes of all echoes at regular intervals. Although this method is not a practicable one for obtaining the complete fading curve of a given echo, it is suitable for obtaining information about the average amplitude and power.

7.3.1. Details of Apparatus.

The four receivers used were of modified Loran type A/APN4 with a band -width of 30 Kc/s and a tuning range from 1.5 to 11.5 Mc/s. They were connected to Admiralty type 96 indicator units, the CR screens of which were photographed with 35 mm. cameras using continuously moving film. The echoes were displayed on a normal type A time base. Nine times per minute the brilliance of the time base was increased sufficient-ly for $\frac{1}{5}$ second to produce a record on the film. The audio and I.F. gains of the receivers were adjusted so that the signal amplitudes displayed on the CR tubes were $\frac{3}{8}$" when overloading of the I.F. channels occurred. Under these conditions the response curves of the receivers were linear up to 2/3 of the indicated overload points. Fig. 50 shows the measured response curves. The transmitter, emitting 100 microsecond pulses at the rate of 50 per second was the same one which has previously been described in section 7.1.4. All the transmitting and recording equipment was normally switched on for two hours daily by time switches.

7.3.2. Calibration of the Receivers-

Since the topographical features of the available receiving sites varied greatly, it was considered that measurement of the absolute value of the echo amplitude was impracticable. The overall gains of the receivers were therefore measured by recording the amplitude of ordinary echoes with reduced transmitter power. Since the amplitude of ordinary echoes was usually between fifty and one hundred times that of Z echoes, the amplitudes of both types could not be recorded at the same time. It was assumed that the average power level of ordinary echoes was the same at all stations, the average Z echo power then being calculated as follows:

$$\frac{\text{Z echo power at A}}{\text{Z echo power at D}} = \frac{(\overline{Amp_Z A})^2 \cdot (\overline{Amp_O D})^2}{(\overline{Amp_Z D})^2 \cdot (\overline{Amp_O A})^2} \qquad (55)$$

Amp_Z = amplitude of Z echoes

Amp_O = amplitude of O echoes

7.3.3. Sampling Technique.

For a given statistical distribution of echo amplitudes we may relate the average value to the average obtained by sampling the fading curve at given intervals. However, for Z echoes the length of the records available has not been sufficient to determine their statistical distribution. This is because the echoes show the characteristic slow fading, usually about two peaks per minute, which would be expected from their narrow angular power spectrum. Superimposed on this is a slow change in average level, usually with a period of between five and fifteen minutes, which may be due to changes in the scattering characteristics of the reflecting layer. Fig.51 shows a typical continuous record of Z echo amplitude obtained with the amplitude recorder attached to the D.F. equipment.

To avoid making any assumptions regarding the statistical distribution of Z echo amplitudes the errors involved in sampling the amplitudes at different rates were estimated, using a typical continuous amplitude record. The results are summarised in Table 5. It can be seen that at the chosen rate of nine samples per minute the errors in finding the averages did not exceed 7.5% for a record length of five minutes.

7.3.4. Measurements.

The amplitude records were measured by enlarging them in a film reader. The errors which occurred during this process were estimated by projecting a typical echo photograph on to plain paper. The r.m.s.

error in measuring the amplitude of the echo forty times independently, was 3.2% of the mean value. For weak echoes the error would be proportionately greater.

TABLE 5.

No. of Samples. 5 minute record	Average Amplitude Arbitrary Units.
484	31.2
45	33.7
30	32.9
15	32.8

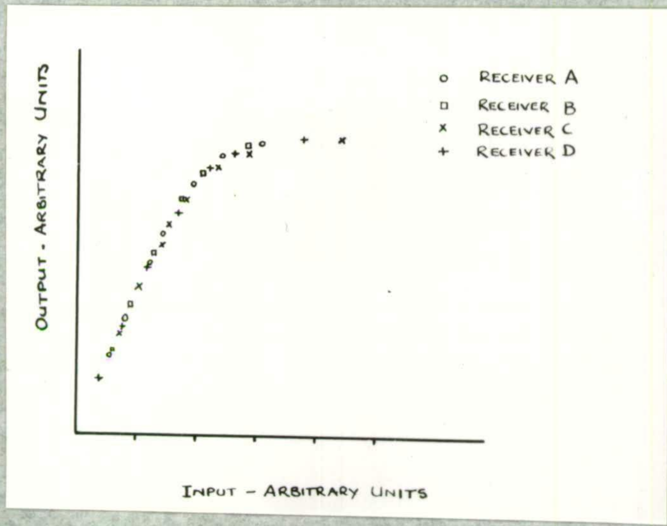

FIG. 50. Receiver Response Curves.

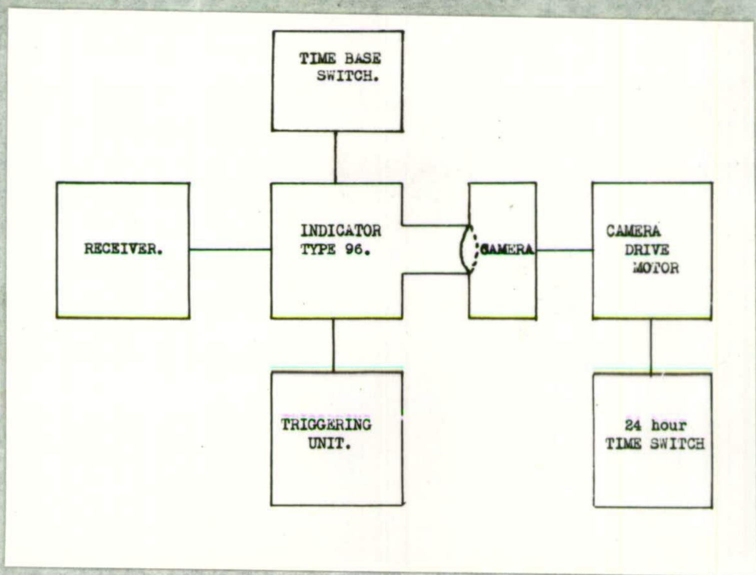

FIG. 51. Block Diagram of Amplitude Recording Equipment.

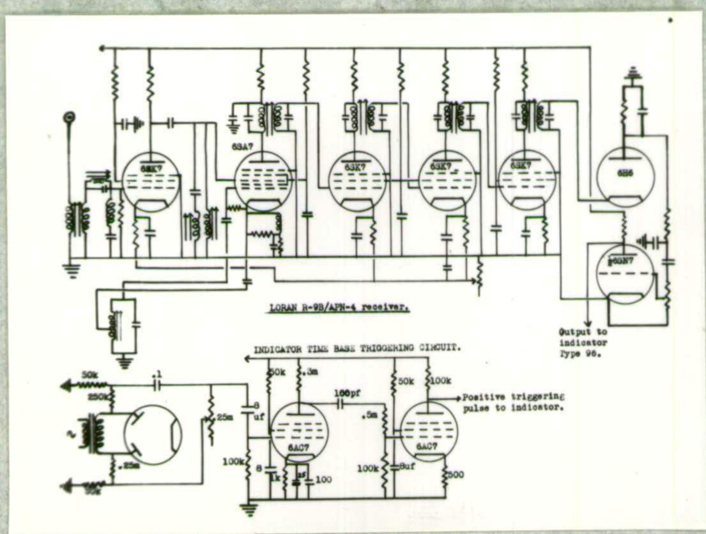

FIG. 51 (a). Circuit of Receiver

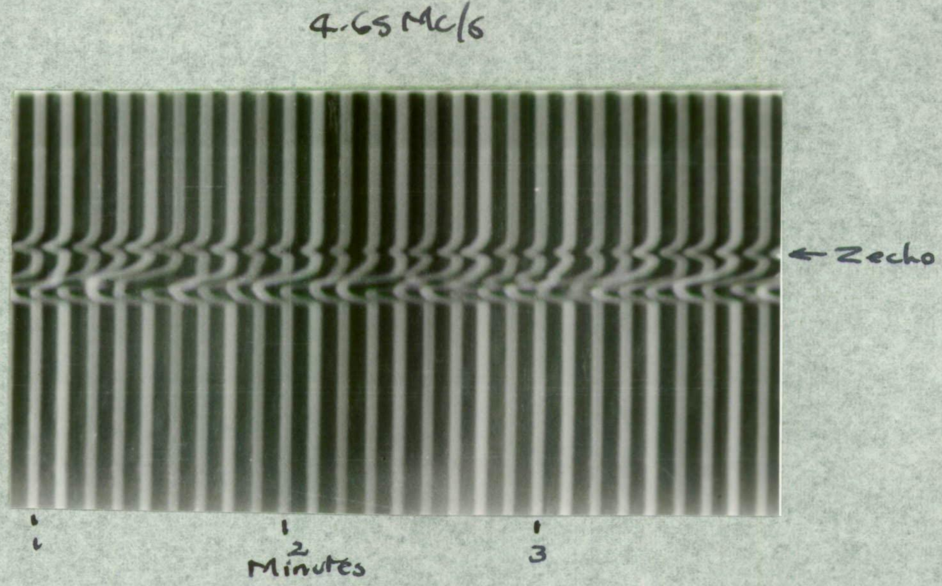

FIG. 52.

Typical Intermittent Amplitude Record,

showing Z Echo.

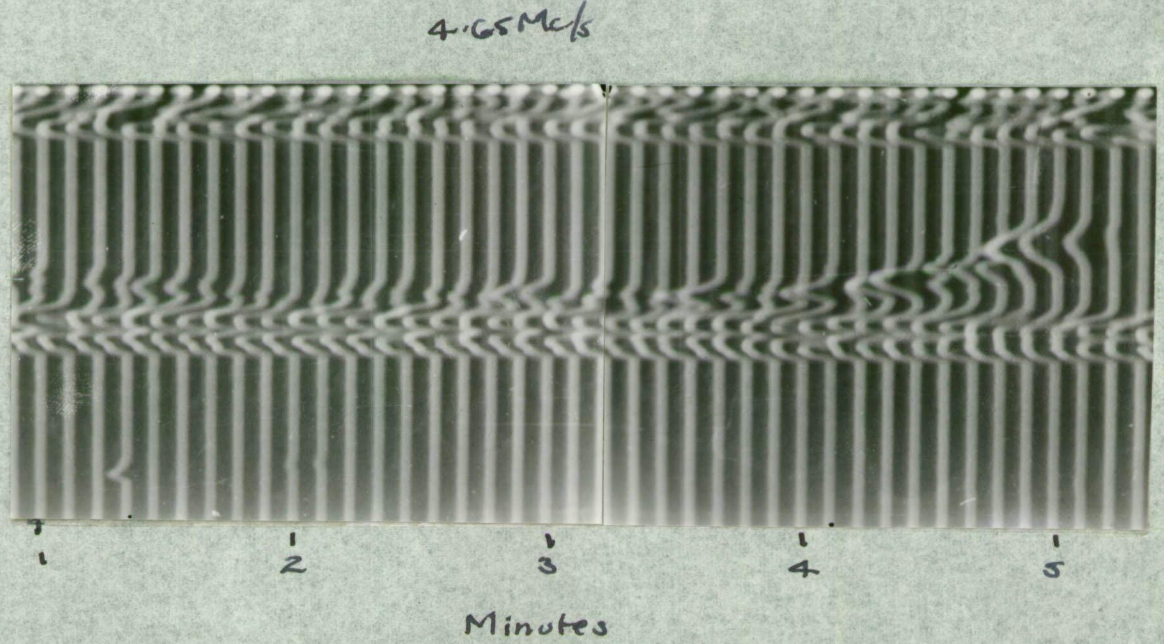

FIG. 53.

Record Showing Increase in Z Echo Amplitude near

the Critical Frequency.

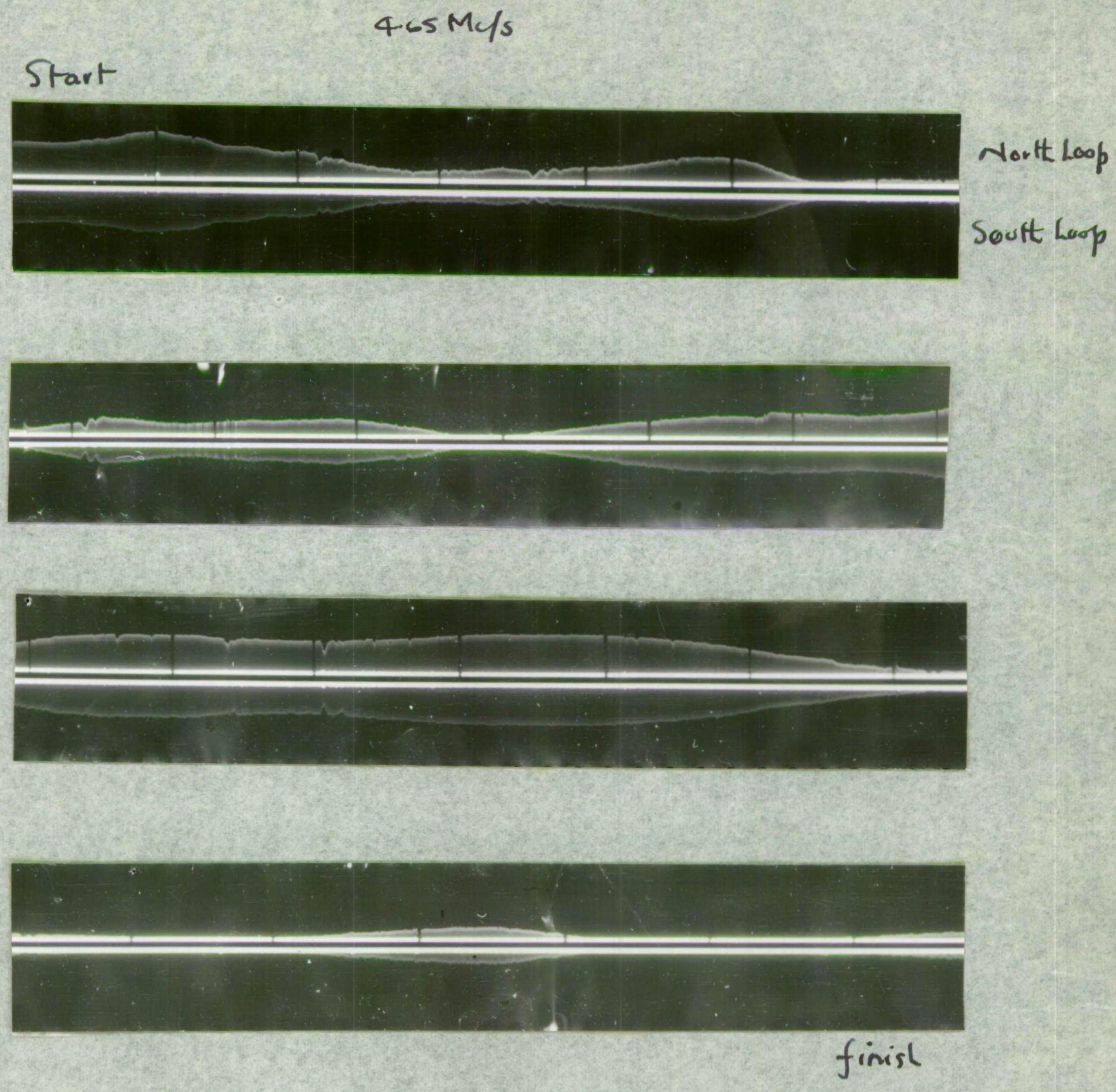

FIG. 54.

Continuous records of Z echo amplitudes obtained, using the twin channel amplitude recorder attached to the D.F. Equipment. Records on each strip refer to the amplitudes at the North and South loops respectively (120' apart) The time marks are 10 seconds apart.

This record shows the typical slow fading of Z Echoes.

8. CONCLUSION.

Measurements of the polarisation and the angle of arrival of Z echoes have been made at Hobart. These led to what is believed to be the correct explanation of F region triple splitting in middle latitudes, namely, that the Z echo results from the back-scattering from the Z reflection level, of ordinary waves which have penetrated the ordinary level of reflection at a certain critical angle of incidence (Ellis (31)).

It followed from the mechanism of occurrence of Z echoes that they should possess the unique property of returning to the ground in a narrow beam. The existence and some of the characteristics of this Z beam were demonstrated by measurements of the amplitude of Z echoes in the vicinity of the transmitter. These measurements led to the concept of a propagation hole in the ionosphere, some applications of which were discussed.

ACKNOWLEDGEMENTS

This work was carried out at the University of Tasmania and at the Mount Nelson Ionospheric Station of the Commonwealth Observatory. The construction of the D.F. equipment was aided by a grant to the University by the Radio Research Board of the C.S.I.R.O. During the period of the investigation the author was employed by the Ionospheric Prediction Service of the Commonwealth Observatory.

The problem of finding an explanation of triple splitting was suggested by Mr. G. Newstead to whom the author is indebted for many helpful discussions. Mr. G. Goldstone assisted in building and operating the amplitude equipment.

REFERENCES

1. ECKERSLEY, T. L. 1933 Proc. Roy. Soc. A141, p.710
2. TOSHNIWAL, G. R. 1935 Nature 135, p.471
3. HARANG, L. 1936 Terr. Mag. Atmos. Elect., 41, p.160
4. MEEK, J. H. 1948 Nature 161, p.597
5. SEATON, S. L. 1948 Proc. Inst. Radio Eng., 36, p.450
6. SCOTT, J.C.W. 1950 J. Geophys. Res., 55, p.65
7. NEWSTEAD, G. 1948 Nature 161, p.312
8. RYDBECK, O. E. H. 1950 J. Appl. Phys. 21, p.1205
9. RYDBECK, O. E. H. 1949 Trans. Chalmers Inst. Tech. No.34
10. BREMMER, H. 1949 Phillips Res. Rep. No.4 , pp.1 and 189
11. WESTFOLD, K. C. 1949 Aus. J. Sci. Res. A.2, p.168
12. DAVIDS, N. 1953 J. Geophys. Res. 58, p.311
13. GERSON, N. C. 1951 Rep. Prog. Phys. 14, p.316
14. TAYLOR, Mary 1934 Proc. Phys. Soc. 46, p.408
15. ECKERSLEY, T. L. 1950 Proc. Phys. Soc. 63, p.49
16. DIEMINGER, W. 1949 Naturwiss 36, p.56
17. HOGARTH, J. E. 1951 Nature 167, p.943
18. LANDMARK, B 1952 J. Atmosph. Terr. Phys. 2, p.254
19. ROSS, W., BRAMLEY, E. N. and ASHWELL, G. E. 1951 Proc. Inst. Elec. Engrs. 98 (Part 111) p.294
20. BOOKER, H. G. 1938 Phil. Trans. Roy. Soc. A237, p.411
21. POEVERLEIN, H. 1949 Zeits. fur Angew. Phys. 1, p.517
22. MOLLER, H. G. 1953 Private Communication from W. Dieminger
23. MACDONALD, D. K. C. 1949 Proc. Camb. Phil. Soc. 45, p.368
24. BRAMLEY, E. N. 1951 Proc. Inst. Elec. Engrs. 98 (Part 111) p.19
25. KELSO, J. M. 1954 J. Atmosph. Terr. Phys. 5, p.11
26. BRIGGS, B. H. and PHILLIPS, G. J. 1950 Proc. Phys. Soc. 63 (Part 11), p.907
27. SHAIN, C. S. and HIGGINS, C. A. 1954 Aust. J. Phys. 7, p.130
28. PULLEY, O. 1935 Proc. Phys. Soc. 47, p.1098
29. ECKERSLEY, T. L. and FARMER, F. T. 1945 Proc. Roy. Soc. A184, p.196

30. BENSON, F. A. and CARTER, A. C. 1950 Electronic Eng. 22, p.238

31. ELLIS, G. R. 1953 J. Atmosph. Terr. Phys. 3, p.263

32. McNICOL, R. W. E. 1949 Proc. Instn. Elect. Engrs. 96 (Part 111), p.517